國 立 交 通 大 學

資訊工程系

碩 士 論 文

使用者輔助的模型化簡

User-Assisted Mesh Simplification

研究生：彭其瀚

指導教授：莊榮宏　博士

中 華 民 國 九 十 四 年 十 月

User-Assisted Mesh Simplification

Student: Chi-Han Peng Advisor: Dr. Jung-Hong Chuang

Department of Computer Science and Information Engineering
National Chiao Tung University

ABSTRACT

Many simplification methods have been proposed to generate multiresolution models for real-time rendering applications. Practitioners have found that these methods fail to produce satisfactory result when models of very low polygon count are desired. This is due to the fact that the existing methods take no semantic or functional metric into account, and moreover, each simplification metric has its own strength and weakness as well in preserving geometric features. To overcome such limitations, we propose an interactive system that allows users to refine unsatisfactory regions on any level of simplification. Our approach consists of two stages. The first stage involves modifying the simplification order to postpone the collapsing for edges in the unsatisfactory regions. The second stage is a local refinement tool aiming to provide fine tuning on the simplified meshes. The major advantage of our approach is that our system provides a predictable and quantifiable control over the refining process. The system is packed as a 3ds Max plugin, so users can easily integrate our system into the digital content creation process.

Keywords: level of detail, mesh simplification, user-assisted simplification.

Acknowledgments

I would like to thank my advisors, Dr. Jung-Hong Chuang, for his inspirations, guidance and patience for the past years.

I also appreciate all my classmates and members of the CGGM laboratory, for their assistances and discussions. Especially, thank Tan-Chi Ho for guidance for this thesis and Chih-Chun Chen for his LOD system framework used in the implementation of this thesis.

I am grateful to my mother, father and my brother for their support, encouragement and love.

Contents

List of Figures

List of Tables

CHAPTER 1

Introduction

1.1 Motivation

Polygonal meshes has become the most common model presentation in 3D computer graphic applications. With the development of 3D scanning technologies and modeling tools, raw meshes can be composed of thousands to millions of polygons. To process such large models efficiently, many mesh simplification algorithms have been proposed to decrease the complexity of models while maintaining similarity with the original model.

Several algorithms have been proposed to derive the so called progressive meshes by using a series of primitive collapsing, such as edge collapsing, in the increasing order of simplification cost. These algorithms usually differ in how the simplification cost is measured. Among others, we list quadric error metric (QEM) [6], appearance preserving simplification (APS) [12] and image driven simplification (IDS) [16]. QEM measures the geometric error between the simplified mesh and original mesh, APS represents the texture deviation resulting from the simplification, and IDS calculates the visual difference. Each of these well known metrics has its own strength and weakness in preserving geometric and texture features. Moreover, all of these metrics do not take semantic or functional features into account. As a result, practitioners have found that these metrics alone are not able to produce satisfactory result when the simplified mesh of low-polygon count are expected.

To overcome such limitations, *user-assisted simplification* has been proposed recently [1] [5] [7] [22]. For example, in user-guided simplification [5] [22], users revise the simplified mesh by re-ordering the simplification order such that edges in the selected region will be collapsed later. The re-ordering of edge collapses is done by multiplying the simplification cost of these edges with a user-specified multiplier. These methods suffer from several problems. For example, the value of the multiplier has no direct relation to the resulting simplification. In consequence, the multiplier is usually chosen in a trial and error basis. Moreover, the appropriate multiplier may be different for different error metrics since the ranges of the different metrics vary greatly.

1.2 Contributions

We propose a user-guided framework that allows users to improve the quality of simplified meshes by existing error metrics, such as QEM and APS. The framework consists of two stages. The first aims to reorder the edge collapse by a weighting scheme. The proposed weighting scheme differs from the previous ones in that the weighting values are automatically derived based on how many more vertices users expect to have in the interested region. The second is a local refinement scheme aims to fine tune the mesh resulting from the first stage.

Our system is packed as a 3ds Max plugin, which offers an easy-to-use user interface and is compatible with existing applications, and in consequence, can be integrated into the digital content creation process.

1.3 Thesis Organization

In chapter 2 we will introduce background and previous work related to this thesis. Chapter 3 presents our user-assisted mesh simplification schemes. In chapter 4 some implementation details and the experimental results will be given, and chapter 5 is the conclusions and discusses of future work.

C H A P T E R 2

Related Work

In this chapter, a review on related work of our method will be given. Section 2.1 introduces the general architecture of level of detail (LOD) modeling. In section 2.2, *progressive meshes* [9], a widely-used continuous presentation of multi-resolution modeling is described. In section 2.3, we will introduce two methods of measuring error of mesh simplification operations. In section 2.4, we will introduce two methods of view-dependent LOD, including view-dependent refinement of progressive meshes [10] and truly selective refinement of progressive meshes [13]. In the last section, we will describe the methods of user-assisted simplification.

2.1 Level-of-detail Modeling

Level-of-detail (LOD) modeling aims to represent a complex mesh with several levels of detail, and from which an appropriate level is selected at run time to represent the original mesh, as shown in Figure 2.1. A number of methods have been proposed in the literature. Most methods simplify the given mesh by using a sequence of primitive reduction operations, such as edge collapse [11], triangle collapse [8], vertex clustering [19], vertex removal [20], and multi-triangulations [4].

The primitive reduction operation can be organized in various orders. The simplest way is to perform the operations in arbitrary order. A more sophisticate approach is to perform the operations in the increasing order of simplification cost, which is analogous to the greedy algorithm.

Several error metrics have been proposed to determine the cost of primitive reduction

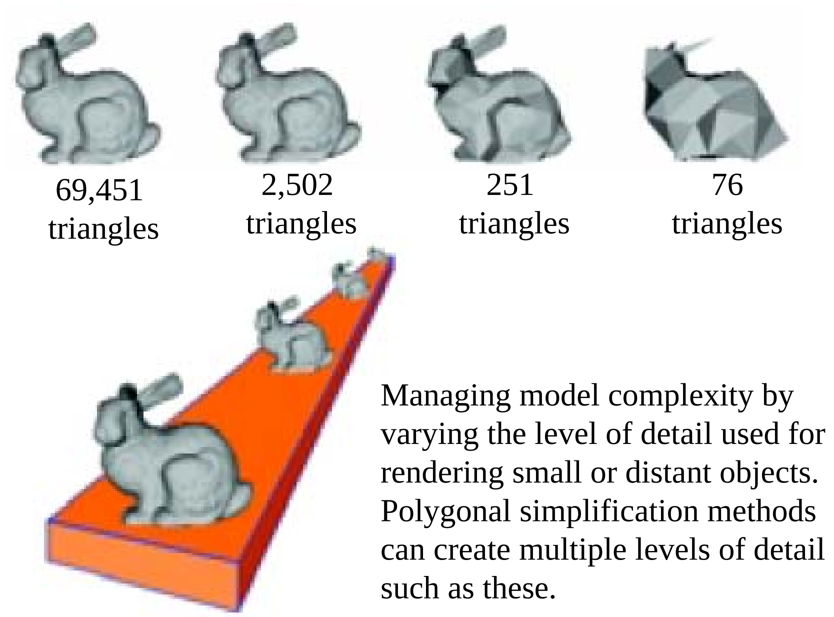

Figure 2.1: The concept of LOD [17].

operation, such as quadric error metrics (QEM) [6], appearance-preserving simplification (APS) [12], image-driven simplification (IDS) [16] and perceptually guided simplification of lit, textured meshes [18]. Different error metric has its strength in preserving certain properties of the original mesh. For example, quadric error metrics aims to preserve the geometric accuracy during the simplification process, and image-driven simplification aims to preserve the visual fidelity between the simplified mesh and the original mesh.

LOD can be *discrete* [3] or *continuous* [9]. Discrete LOD creates various levels of detail for the original mesh, each of which has no direct relation to others and cannot be derived from other levels. At run-time, an appropriate level of detail is chosen to present the original mesh. On the other hand, continuous LOD creates a data structure encoding a continuous spectrum of detail so that at run-time the desired level of detail can be extracted from this structure. The progressive meshes, which will be described in section 2.2, is an example of continuous LOD.

Continuous LOD can also be *view-independent* or *view-dependent* [10]. In view-independent LOD, the extraction of level-of-detail does not consider the viewing parameter, resulting in a mesh of uniform resolution. But in view-dependent LOD, the current viewing parameter and screen error of the primitive reduction are considered in the run-time extraction of level of detail such that the mesh resolution will be nonuniform, depending not only on the surface geometry but also in visibility and where the focus point is. We will describe two methods of view-dependent LOD in section 2.4.

2.2 Progressive Meshes (PM)

As a continuous multi-resolution representation of triangular meshes, the progressive meshes (PM) [9] consists of a base mesh and a sequence of vertex split operations which is the inverse sequence of edge collapses and are used to refine the base mesh. In PM construction, a given mesh is simplified by a sequence of edge collapses until no more edge collapses are possible. Each edge collapse removes a vertex and two faces from the mesh, while its inverse operation, called *vertex split*, adds a vertex and two faces to the mesh. Figure 2.2 shows the behavior of an edge collapse and its corresponding vertex split.

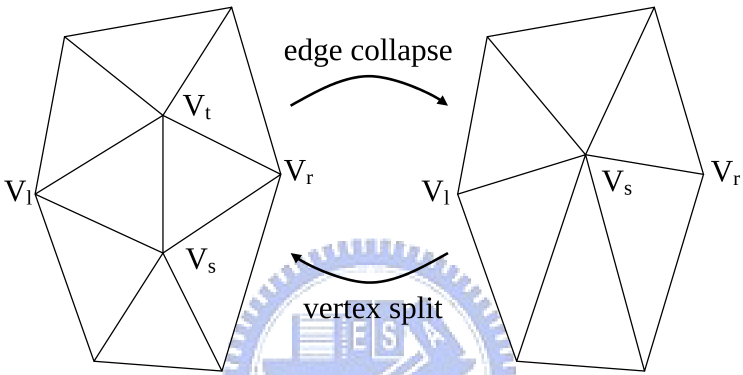

Figure 2.2: Edge collapse and vertex split [9].

Given an input mesh M and a sequence of n edge collapses, a PM sequence with $n+1$ levels of detail is constructed. As shown in Figure 2.3, starting at M_5, the application of five edge collapses results in a PM of six levels, in which the mesh of the simplest level is denoted as M_0. Executing the $(i-1)$-th edge collapse, called $ecol_{i-1}$, on M_i will bring out M_{i-1}, and executing the (i)-th vertex split, called $vsplit_i$, on M_i will bring back M_{i+1}.

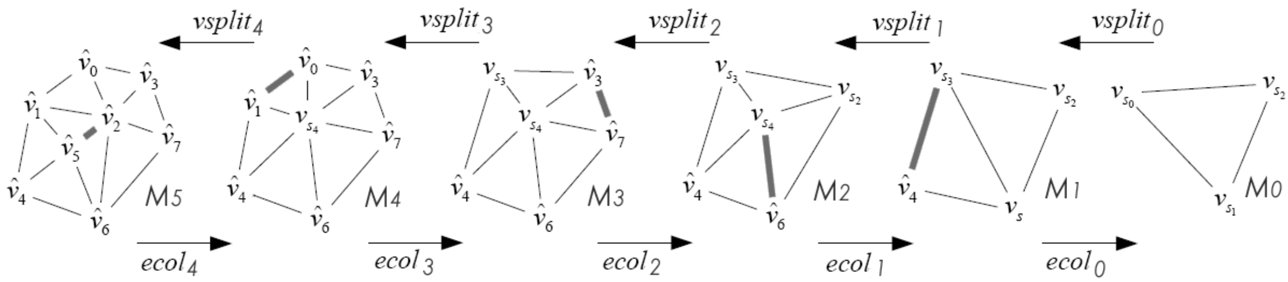

Figure 2.3: PM sequence [14].

The PM sequence is constructed using greedy algorithm. First, all possible edge collapses over the input mesh are collected as candidates, then the *cost* of each candidate is calculated, and finally the edge collapse is executed in the order of increasing cost. After each edge collapse, the costs of remaining candidates shall be updated and invalid records, i.e, edge collapses with nonexist V_u or V_v, are removed from the candidate list. Such a cost update is time consuming and can be delayed using lazy evaluation as proposed in [6].

2.3 Error Metrics

The cost of the edge collapse can be approximated by a number of error metrics, such as geometric error metrics (QEM) [6], appearance-preserving simplification [12] and image driven simplification [16]. In this section we will briefly describe QEM and APS.

2.3.1 Quadric Error Metrics (QEM)

QEM approximates the cost of each edge collapse as the distances from the neighboring faces of the original vertices V_u and V_v to the new vertex V. To do this, the first thing is to evaluate the total distance of a vertex v to its neighboring faces by

$$\triangle(v) = \sum_{p \in \mathrm{NF}(v)} (p^T v)^2, \tag{2.1}$$

where $v = [v_x \ v_y \ v_z \ 1]^T$, $\mathrm{NF}(v)$ is the set of v's neighboring faces, and $p = [a \ b \ c \ d]^T$ representing the plane defined by $ax + by + cz + d = 0$ where $a + b + c + d = 1$. Equation 2.1 can be rewritten as the following quadratic form

$$\triangle(v) = \sum_{p \in \mathrm{NF}(v)} (vp^T)(pv^T) = \sum_{p \in \mathrm{NF}(v)} v^T(p^T p)v = v^T(\sum_{p \in \mathrm{NF}(v)} K_p)v, \tag{2.2}$$

where K_p is called the fundamental error metric for plane p, and can be presented in 4x4 matrix form as

$$K_p = p^T p = \begin{bmatrix} a^2 & ab & ac & ad \\ ab & b^2 & bc & bd \\ ac & bc & c^2 & cd \\ ad & bd & cd & d^2 \end{bmatrix}. \tag{2.3}$$

Let $Q(V)$ denotes $\sum_{p \in \mathrm{NF}(v)} K_p$, presenting the total distances of v to its neighboring faces. $Q(v)$ is called the *quadric error metric (QEM)* of v.

To evaluate the cost of an edge collapse $(V_u, V_v) \rightarrow V$, $Q(V_u)$ and $Q(V_v)$ are summed as V to approximate the total distance of V to the neighboring faces of V_u and V_v. By replacing $(\sum_{p \in \mathrm{NF}(v)} K_p)$ by $Q(V)$ in Equation 2.2, we have the cost function of edge collapse $(V_u, V_v) \rightarrow V$ as

$$\triangle(V) = V^T Q(V) V. \tag{2.4}$$

As you can see in Equation 2.3.1 that the cost of each edge collapse is heavily influenced by the position of V. We can find the optimal position of V by minimizing $\triangle(V)$. Because the cost function $\triangle$ is quadratic, the minimum value can be found by solving the linear system $\partial\triangle/\partial x = \partial\triangle/\partial y = \partial\triangle/\partial z = 0$, that is

$$\begin{bmatrix} Q_{11} & Q_{12} & Q_{13} & Q_{14} \\ Q_{21} & Q_{22} & Q_{23} & Q_{24} \\ Q_{31} & Q_{32} & Q_{33} & Q_{34} \\ 0 & 0 & 0 & 1 \end{bmatrix} V = \begin{bmatrix} 0 \\ 0 \\ 0 \\ 1 \end{bmatrix}$$

where Q_{ij} is the (i, j)-th element of $Q(V)$. If the coefficient matrix is not invertible, we just pick among the positions of V_u, V_v or $(V_u + V_v)/2$ that has the least cost.

While building the PM sequence, the QEM of each vertex that affected by an edge collapse need to be updated accordingly. The QEM of each remaining vertex during the PM building phase approximates the total distances from the vertex to all the faces collapsed to it.

2.3.2 Appearance-Preserving Simplification

Cohen et al. introduced the appearance-preserving simplification (APS) in 1998 [12], which considers *texture deviation* as the simplification error of an edge collapse. As can be seen in Figure 2.4, texture deviation is the geometric distance between two points that correspond to the same texture coordinate. To evaluate the cost of an edge collapse, Cohen et al. considered the maximum of the texture deviation occurred on the collapsed polygons, which are the neighboring faces of the collapsed vertex.

To efficiently sample texture deviation over the collapsed faces of an edge collapse, we need to find the overlay of these faces in the texture domain. Figure 2.5(a) shows such an example, where solid lines and dot lines represent the overlay before and after the edge collapse, respectively. The edges on the overlay partition the region into a set of convex,

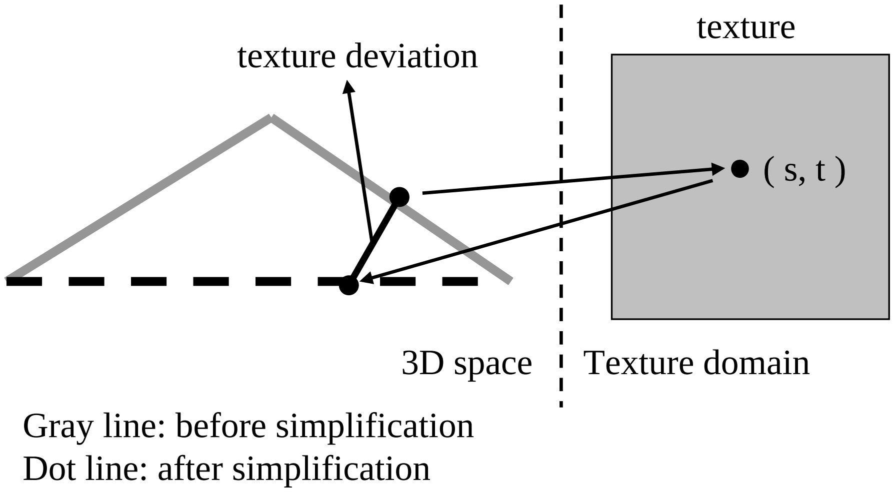

Figure 2.4: APS Texture deviation [15].

polygonal *mapping cells* (each identified by a grey dot in Figure 2.5(b)). Since the texture deviation varies linearly on each mapping cell, the maximum texture deviation can only be found on the boundary vertices of mapping cells (identified by red dots in Figure 2.5(b)).

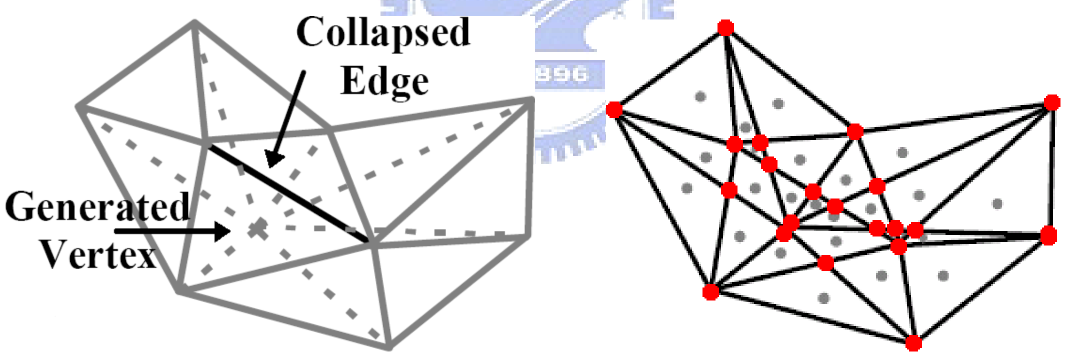

(a) Overlay in the texture domain before and after an edge collapse.

(b) Mapping cells (identified by grey dots) and sampling positions (identified by red dots).

Figure 2.5: Sampling the texture deviation [12].

The global texture deviations can be approximated by using a set of axis-aligned bounding boxes. In Figure 2.6(a), the original mesh M_0 is simplified to M_i consisting of two segments, and the rectangle representing the bounding box of the segment bounds the maximum texture deviation for the simplification from M_0 to that segment. In Figure 2.6(b), when M_i is simplified to M_{i+1}, the bounding box for M_{i+1} must bound the bounding boxes of the two segments in M_i.

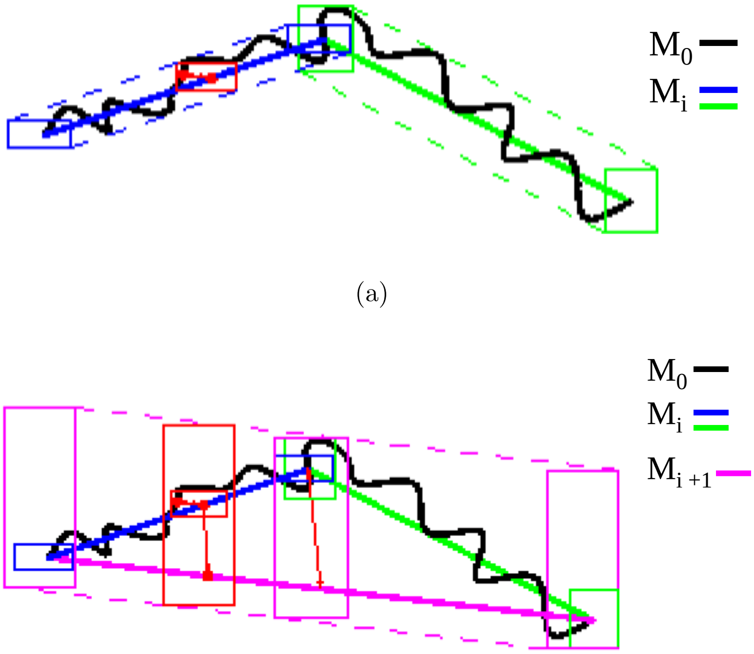

(b)

Figure 2.6: Approximates global texture deviation using bounding box. [12].

2.4 View-Dependent LOD

2.4.1 View-Dependent Refinement of Progressive Meshes

View-dependent LOD modeling aims to support selective refinement, in which the mesh resolution is determined by whether the polygons are back facing or front facing, inside or outside the view volume, and finally the screen space geometric error of the edge collapse. As shown in Figure 2.7, mesh outside the view frustum is severely simplified while mesh within the view volume is kept in higher resolution.

To support view-dependent selective refinement, Hoppe proposed the *vertex hierarchy*, which is a binary forest constructed from the PM sequence. As shown in Figure 2.8, each node in the vertex hierarchy represents a vertex at some level of detail, and each parent-children relation represents an edge collapse record, where the parent representing the new vertex V and the two children are the collapsed vertices V_u and V_v. An *active cut* on the vertex hierarchy represents a selectively refined mesh through the hierarchy, such as M^0 and $\hat{M}$ (the original mesh) in Figure 2.8.

In Hoppe's vertex hierarchy, it is not always legal to execute an edge collapse or a vertex split picked on the active cut unless some *preconditions* are satisfied.

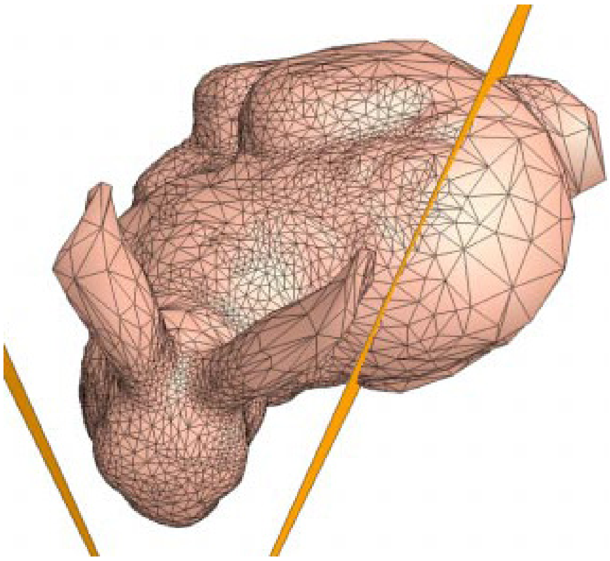

Figure 2.7: View-dependent PM [10].

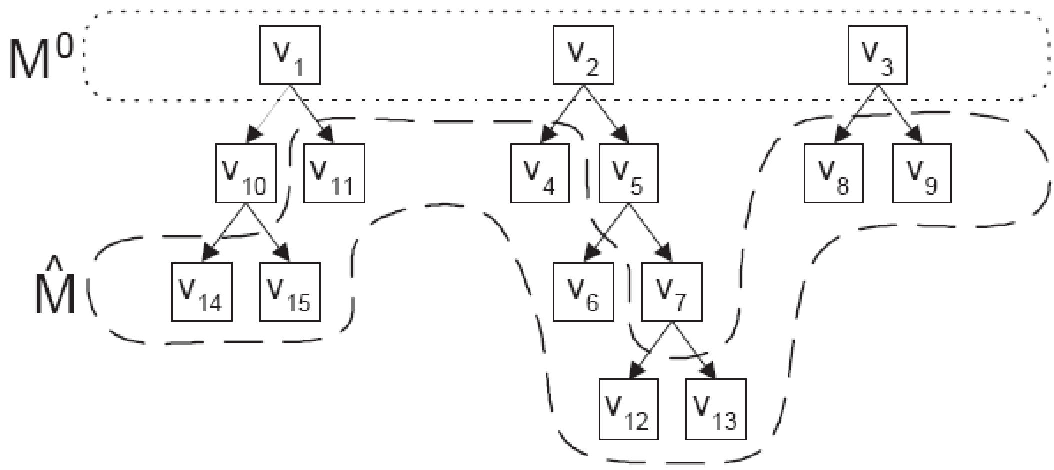

Figure 2.8: Vertex hierarchy [10].

As shown in Figure 2.9, a vertex split is legal if

1. V exists on the current simplified mesh, and
2. The faces f_{n0}, f_{n1}, f_{n2} and f_{n3} are faces that exist on the current simplified mesh.

and an edge collapse is legal to execute if:

1. V_u and V_v exist on the current simplified mesh, and
2. The faces adjacent to f_l and f_r are exactly f_{n0}, f_{n1}, f_{n2} and f_{n3}.

Before executing a vertex split on the active cut for which not all f_{n0}, f_{n1}, f_{n2} and f_{n3} exist on the current simplified mesh, it is necessary to execute vertex splits that will bring

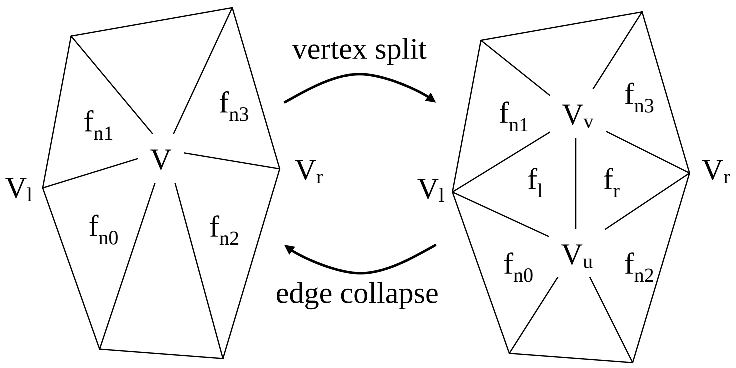

Figure 2.9: Neighboring configurations of edge collapse and vertex split [10].

back the missing faces, and this must be done in a recursive manner. Such phenomenon is called *vertex split dependency problem.* As illustrated in Figure 2.10, the base mesh M^0 is obtained by the edge collapse sequence $ecol_5$, $ecol_4$, $ecol_3$, $ecol_2$ and $ecol_1$. To split the vertex V_5 on M^0, V_4, V_3, V_2 and V_1 must be split in prior.

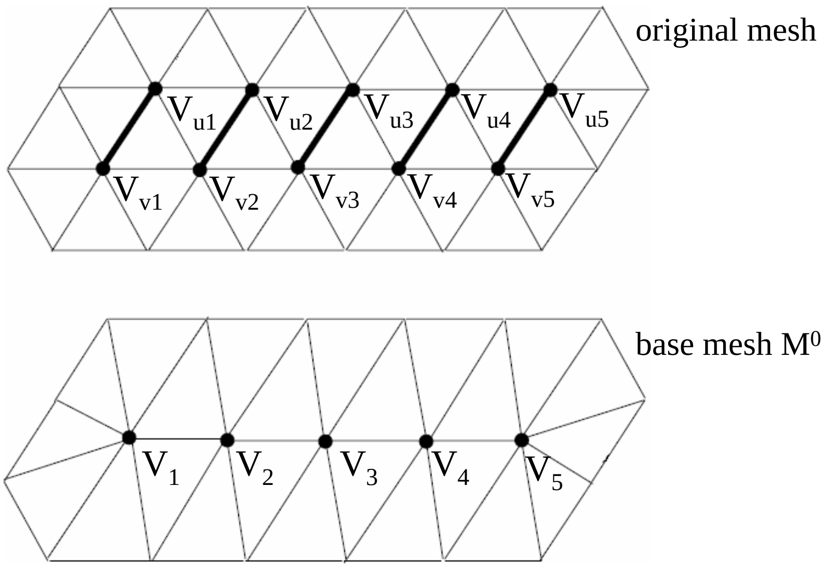

Figure 2.10: Vertex splits dependency problem [13].

2.4.2 Truly Selective Refinement of Progressive Meshes

The vertex split dependency problem has been recently resolved by the truly selective refinement of progressive meshes proposed in [13]. In the truly selective refinement scheme, it is always legal to execute an edge collapse or vertex split chosen from the active cut of the vertex hierarchy, regardless of the configuration of the neighborhood. This is made possible by using new definitions of edge collapse and vertex split, based on the concept of *dual pieces*. Figure 2.11 explains the concept of dual pieces. Figure 2.11(a) shows a subtree in the vertex hierarchy where $\hat{v}_0$, $\hat{v}_1$,...and $\hat{v}_6$ are vertices on the original mesh that are collapsed to a single vertex v_{12}, as shown in Figure 2.11(b). Figure 2.11(c) shows the dual piece of v_{12}, denoted as $D(v_{12})$, on the original mesh, which is an enclosed region including all leaf nodes in the subtree of v_{12}.

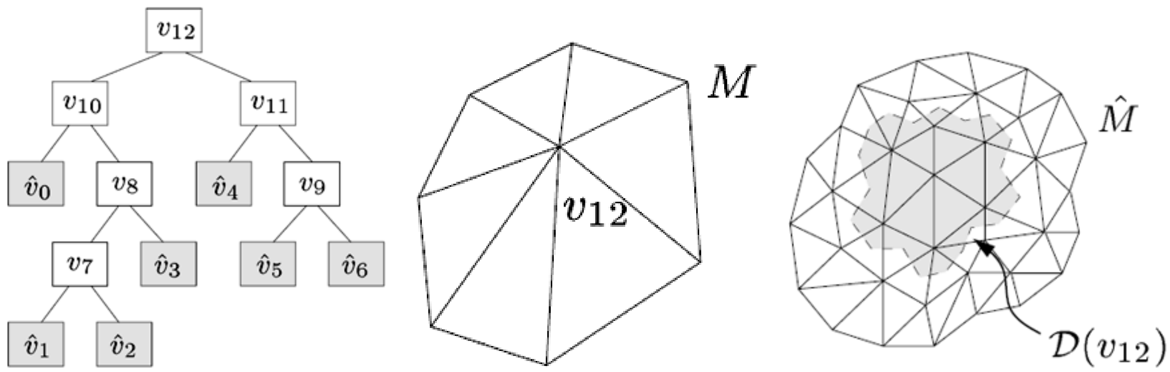

(a) A subtree of v_{12} in the vertex hierarchy.

(b) The simplified mesh where $\hat{v}_0$,...,$\hat{v}_6$ are all collapsed to v_{12}.

(c) The dual pieces of v_{12} on the original mesh.

Figure 2.11: Dual pieces [13].

For a dual pieces in the vertex hierarchy, the following properties hold:

- $D(V) = D(V_u) \bigcup D(V_u)$, $D(V_u) \bigcap D(V_v) = \emptyset$, and $D(V_u)$ and $D(V_v)$ are adjacent to each other for any edge collapses $(V_u, V_v) \rightarrow V$.
- $D(V_q) \subset D(V_p)$ if V_p is an ancestor of V_q in the vertex hierarchy.
- $D(V_p) \bigcap D(V_q) = \emptyset$ if V_p and V_q have no ancestor-descendent relationship in the vertex hierarchy.

According to the the properties described above, Kim et al. defined a set of vertices V to be a valid cut in the vertex hierarchy if it satisfies the following properties, as shown in Figure 2.12:

- The dual pieces of all vertices in V cover the original mesh $\hat{M}$ without overlaps and holes.
- The dual pieces of all vertices in V are simply connected. That is, any two adjacent dual pieces share only one portion of their boundaries.

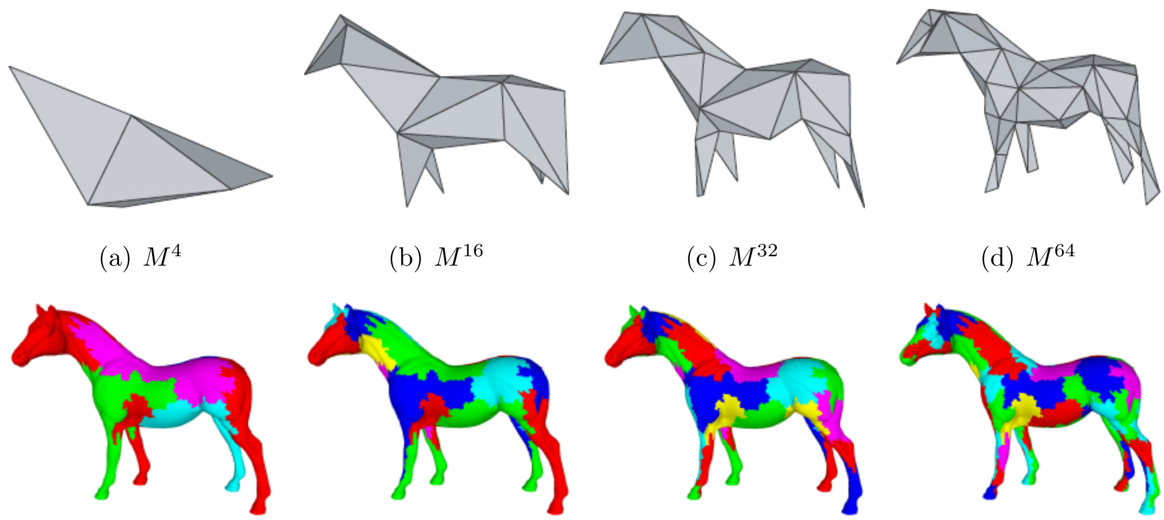

(a) M^4 (b) M^{16} (c) M^{32} (d) M^{64}

(e) Dual pieces of M^4 (f) Dual pieces of M^{16} (g) Dual pieces of M^{32} (h) Dual pieces of M^{64}

Figure 2.12: PM sequence and the corresponding dual pieces [13].

Back to the problem of designing new definitions for edge collapse and vertex split that are free of dependency problems. According to Figure 2.9, vertex V_l and V_r need to exist before we execute the vertex split because it would be impossible to form F_l and F_r without V_l and V_r, which is exactly the vertex split dependency problem. But if we can find vertices to replace V_l and V_r such that the resulting set of vertices still satisfy the properties for a valid cut, we have solved the vertex split dependency problem.

The replacement vertex for inactive V_l or V_r is found to be the active ancestor of the inactive V_l or V_r's *fundamental cut vertex*, which is recorded as follows:

- At startup, the fundamental cut vertex of each vertex is itself.
- For each edge collapse $(V_u, V_v) \rightarrow V$, we label the fundamental cut vertex of V to be V_u.

Kim had proven the correctness of such V_l and V_r replacement scheme in his thesis [14].

2.5 User-Assisted Mesh Simplification

In this section, we will describe several approaches that allow users to intervene the simplification process for better simplification results.

2.5.1 Zeta: a Resolution Modeling System

The first system that allows users to adjust the simplification results is *Zeta* proposed by Cignoni et al. [1]. It requires a pre-computed sequence of primitive simplifications as an input. Zeta utilizes *hyper-triangulation model*, which uses vertex decimation as the local mesh reduction operator. The vertex decimation operator is shown in Figure 2.13, where one vertex is decimated in one simplification step, and the patches associated with the vertex are "glued" onto the common border.

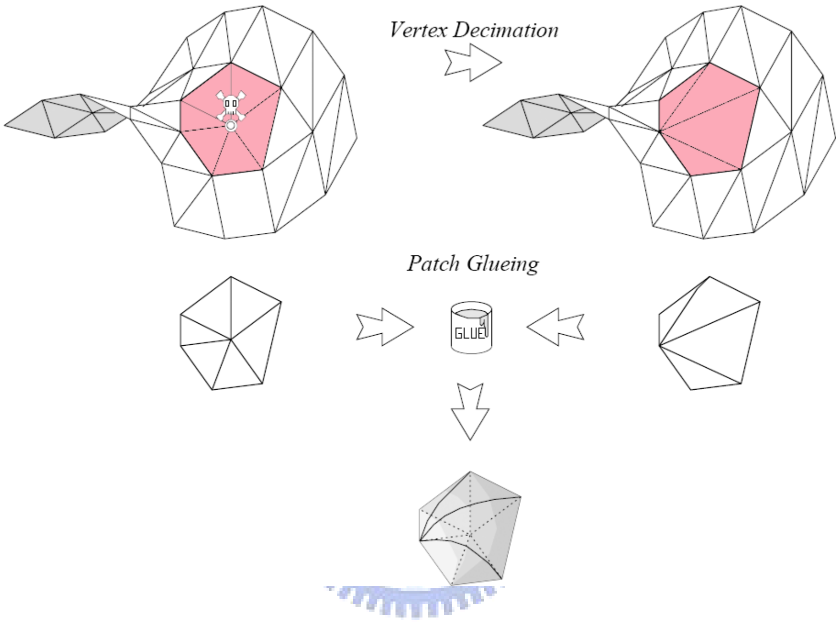

Figure 2.13: Zeta's vertex decimation operator [1].

Users can selectively refine a model by locally changing error thresholds to extract different approximations that did not appear during the original simplification process. As shown in Figure 2.14, a color ramp (red-to-blue) represents the distance from the *focus point* specified by the user. The error threshold is in proportion to how far the distance is, so that the resolution of faces near the focus point is higher then that for faces far from the focus point.

2.5.2 Semisimp

The second approach for user-assisted mesh simplification is *Semisimp* proposed by Li et al [7]. Semisimp proposes three approaches for users to manipulate the simplification results. The first approach is *order manipulation*, in which users can adjust the distribution of detail on simplified models by changing the traversing order of the vertex hierarchy.

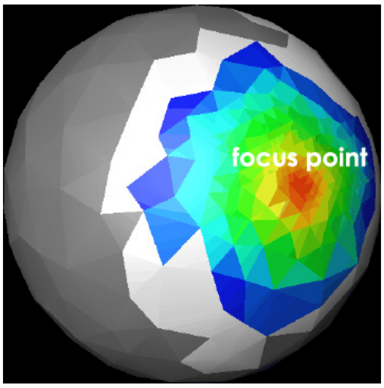

Figure 2.14: Selective refinement in Zeta [1].

The second approach is *geometric manipulation*, in which users can change the positions of vertices in the current cut by dragging the mouse. To maintain smoothness in the current cut and across different levels of detail, changes in position can be propagated to topological neighbors in the current cut, as well as to ancestors and descendants of the affected nodes in the cut. The effect of geometric manipulation is shown in Figure 2.15.

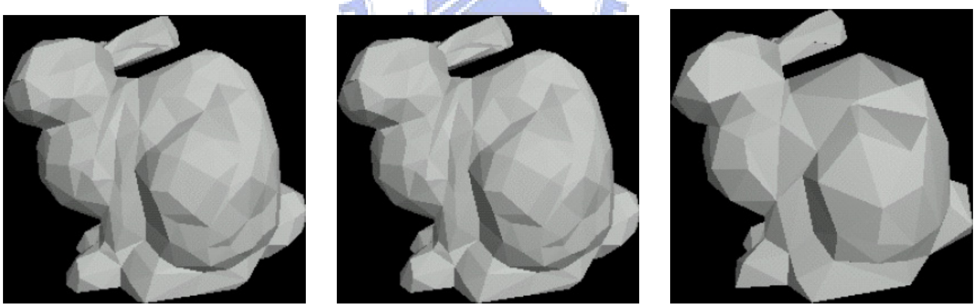

(a) The manipulated level of detail (b) Effects on higher level of detail (c) Effects on lower level of detail

Figure 2.15: Geometric manipulation in Semisimp [7].

The third approach is *hierarchy manipulation*, in which users can also manipulate the vertex hierarchy in the fashion of constructing a subtree containing the user-defined region only, aiming to isolate the simplification sequence on the user-defined region. Figure 2.16 shows an example of hierarchy manipulation in which the user identifies nodes A, B and C as a separated region, and a subtree containing A, B and C is formed after the reconstruction.

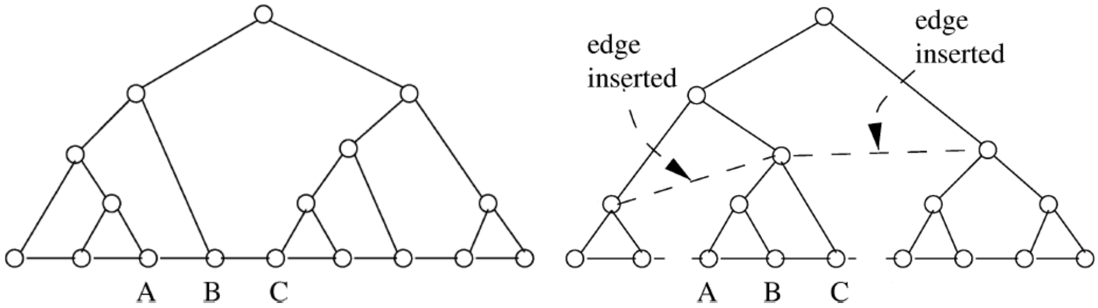

(a) The original vertex hierarchy (b) The reconstructed vertex hierarchy

Figure 2.16: Hierarchy manipulation in Semisimp [7].

2.5.3 User-Guided Simplification

Based on the popular QEM metric, Kho et al. introduced two approaches for users to intervene and control the simplification process [22]. The first approach is *adaptive weighting of quadrics*, in which users can specify weighting multipliers over vertices on the original mesh to change the distributions of quadric error metrics. By weighting the costs over interested regions, the edge collapse operations over these regions will be delayed, and the regional quality will arise. The effect of adaptive weighting of quadrics is shown in Figure 2.17, where weighting multipliers are specified on the eyes and the lips. The weighted regions get improved significantly after the weighting process.

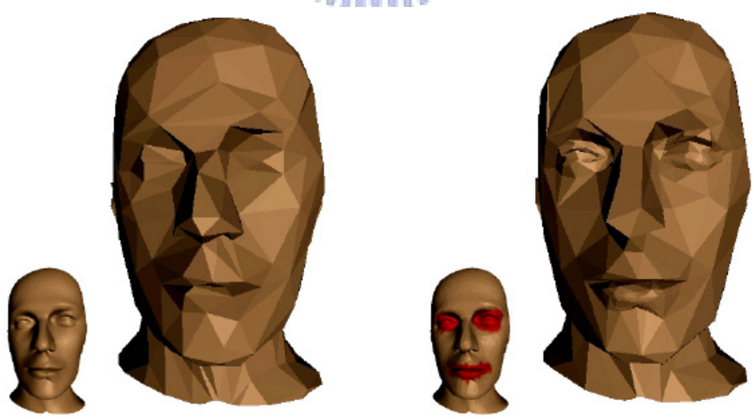

Figure 2.17: The effects of adaptive weighting of quadrics [22].

The second approach is *constraint quadrics*, in which quadric error metric values, instead of multipliers, are added to the vertices on the interested regions by augmenting additional constrained planes. The added constraint quadrics will pull the optimal positions for an edge collapse to the constrained planes.

There are three kinds of constraint quadrics: contour constraints, plane constraints and point constraints. When using contours constraints, first the user selects a contour on the original mesh that shall be preserved. For each edge in the selected contour, two planes running through the edge and perpendicular to each other are generated, then the quadrics of these planes are added to the endpoints of the edge. The added constraint quadrics will pull the optimal position onto the contour edges. Consequently, it preserves the shape of contours. An example of contour constraints is shown in Figure 2.18.

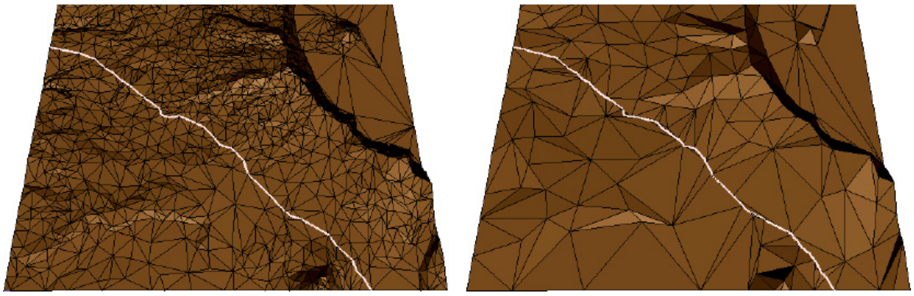

Figure 2.18: An example of contour constraints [22].

On the other hand, plane constraints are designed to be applied to areas that the user wants to preserve as flat regions. When the user selects a set of vertices, a least squares best fit plane to this set is computed, then the quadric of the plane is added to the selected vertices.

Point constraints are added to vertices that the user want to preserve their positions. Point constraints are computed as the sum of quadrics of three planes running through each vertex, where the planes are parallel to the coordinate planes.

In the same year, Pojar et al. also presented an approach for users to refine simplifications [5]. Their approach is very similar to the adaptive weighting of quadrics method, but a Maya plugin is provided, which offers rich UI and great compatibility with other modeling applications.

CHAPTER 3

User-Assisted Mesh Simplification

In this chapter, we will explain the proposed framework for user-assisted mesh simplification. In section 3.1, an overview of our approach will be given, then the weighting approach is described in section 3.2, and section 3.3 explains the the local refinement approach.

3.1 Approach Overview

Current automatic mesh simplification algorithms may perform poorly when a reduced mesh of very low polygon count is desired. To remedy this problem, we provide a two-stage approach that allows users to modify the order of edge collapses and result in better quality in interested regions. The first stage is a weighting scheme that aims to reorder the PM sequence by increasing the cost associated with vertices in the interested regions, leading to the delay of some edge collapses and resulting in higher mesh resolution. Such a cost increase is determined by user-specified inputs, so is different from previous weighting methods. The second stage provides a local refinement scheme that allows users to effectively fine tune the simplification using vertex hierarchy.

Both stages have their own strength. For example, the weighting scheme is more effective in overall refinement over a larger region, but is less effective for fine tuning the simplification. Moreover, the weighting scheme lacks an effective control on where to get polygon budget to maintain a fixed polygon count, and hence may produce unexpected sacrifice in some regions when applied to a model of very low polygon count. On the other hand, the local refinement stage is effective in performing refinements over small areas and recovering sharp features. In the mean time, the local refinement has relatively more control on where to get polygon budget, and hence can be applied to models with very low polygon count.

Figure 3.1 depicts an overview of our framework. At startup, we build a PM sequence from the input mesh using an automatic mesh simplification algorithm, such as QEM [6] or APS [12], and a simplified mesh is retrieved from the PM sequence. If the user is not satisfied with the quality of the simplified mesh, he or she can use weighting scheme to refine large regions and then use local refinement to fine tune small regions or to recover sharp features. The refinement process can be repeated until the user is satisfied with the simplification.

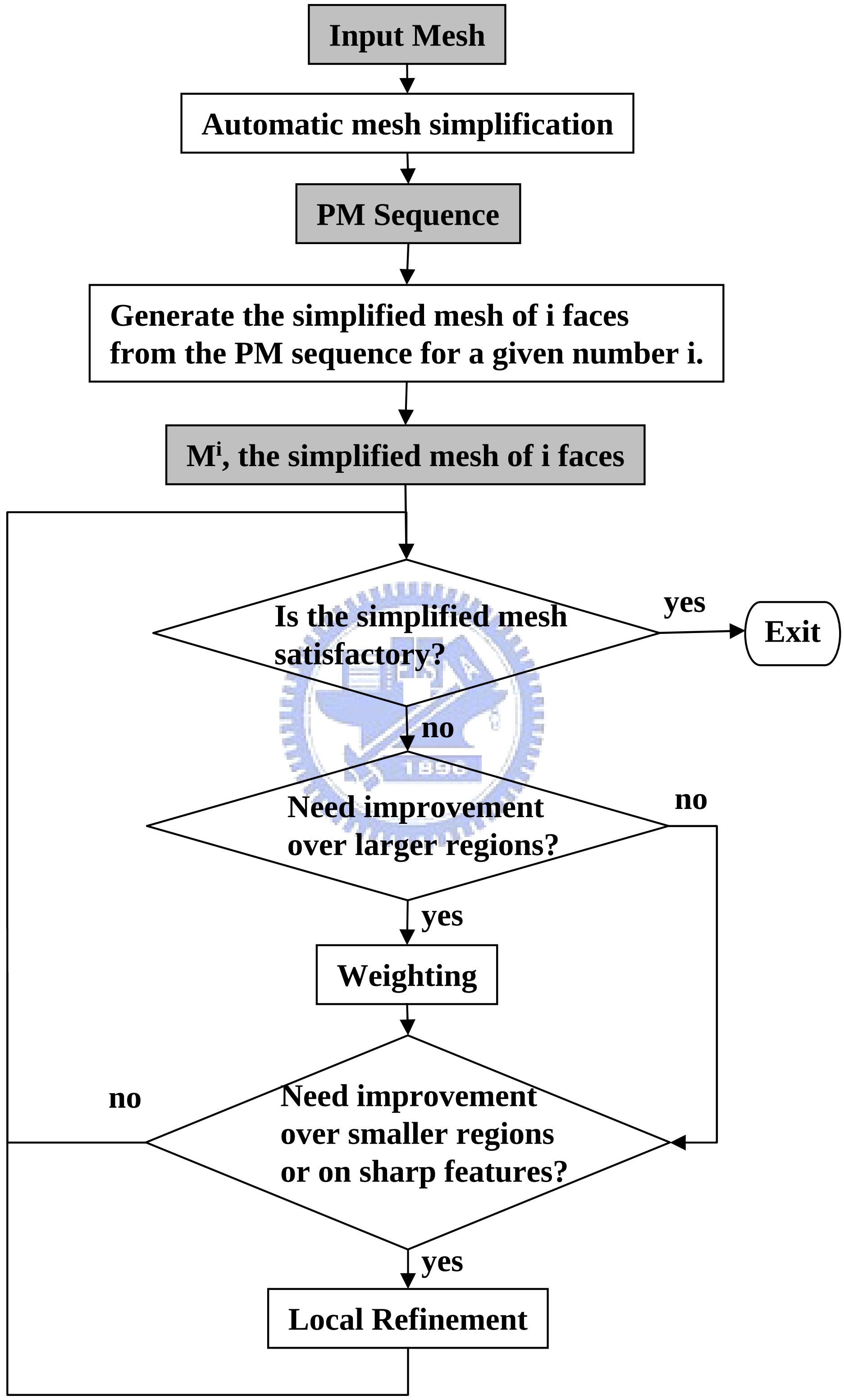

Figure 3.1: System overview.

3.2 Weighting Simplification Cost

Former weighting schemes proposed by Kho et al. [22] and Pojar et al. [5] increase mesh resolution in the interested region by directly multiplying the cost of edge collapse in the interested region with a user-specified multiplier. However, such method has two shortcomings. First, because the value of the multiplier has no direct relation to the resulting simplification, the multiplier is usually chosen in a trial and error basis. Second, for some error metrics, such as QEM, the cost of edge collapse grows rapidly later in the PM sequence, so the effect of multiplying the costs with a multiplier will diminish when simplified to low polygon counts.

The proposed weighting scheme differs from the previous methods in that the weighting values are automatically derived based on how many more vertices users expect to have in the interested regions [1]. No multiplier needs to be specified, what the user needs to input is the number of vertices he or she expects in a region. As a consequence, such a weighting scheme is equally effective for a reduced model of any polygon count.

The basic concept of our weighting scheme is to shift the execution order of all edge collapses in the interested region [2], so that a user-expected number of vertices will be allocated in that region after the model is simplified to a user-specified simplification target. Let's assume that the user-specified simplification target is N vertices, the number of vertices in the interested region is C when the model is simplified to N vertices, and, moreover, the user-expected number of vertices to be allocated in the interested region is C^*.

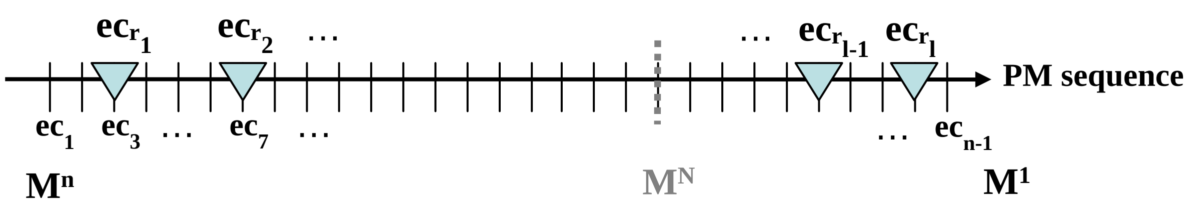

Figure 3.2: Notations of the weighting scheme.

For a given original mesh M^n of n vertices, let's denote all the edge collapses from the original mesh M^n to the most simplified mesh M^1 (consisting of one vertex) are ec_1, ec_2,...,ec_{n-1}, and among them the edge collapses in the interested region are ec_{r_1},

[1] each region is identified as a set of vertices in the original mesh

[2] an edge collapse is in a region if it collapses some vertices belong to that region

ec_{r_2},...,ec_{r_l}, where l is the number of original vertices in that region. The above notations are illustrated in Figure 3.2, where the horizontal line presents the execution order of edge collapses along the PM sequence and triangular dots mark edge collapses in the interested region.

For a given simplified mesh M^N, $N < n$, the weighting scheme consists of two steps. In the first step, the new execution order of ec_{r_1},...,ec_{r_l} are determined, and in the second step, we adjust the simplification cost of these edge collapses so that these edge collapses will be executed at the desired order when the original mesh is re-simplified. The two steps are stated as follows:

1. Shift the execution order of ec_{r_1},ec_{r_2},...ec_{r_l} such that there are C^* edge collapses $ec_{r_{(l-C^*+1)}}$,...,ec_{r_l} avoid to be performed when the original mesh is re-simplified to M^N. Because the number of remaining vertices in the interested region is determined by the number of edge collapses not are not yet performed in the region, by doing so we can assure that there will be C^* vertices allocated in the interested region after the original mesh is re-simplified to M^N. This stage involves

   (a) Find the new place where $ec_{r_{(l-C^*+1)}}$ is shifted to. Since the given simplified mesh, M^N of N vertices, is obtained by doing edge collapses ec_1, ec_2,...,ec_{n-N-1}, the edge collapse $ec_{r_{(l-C^*+1)}}$ shall be shifted to the place for $ec_{n-N+(C^*-C)}$. Doing so, we will assure that there will be C^* edge collapses in the interested region that are not yet performed after the original mesh is re-simplified to M^N. This stage is illustrated in Figure 3.3.

   (b) Shift all edge collapses ec_{r_1}, ec_{r_2},...,$ec_{r_{(l-C^*)}}$,$ec_{r_{(l-C^*+2)}}$,...,ec_{r_l} in a magnitude similar to that for $ec_{r_{(l-C^*+1)}}$. One way to do this is as follows:

      - For each of ec_{r_2},...,$ec_{r_{(l-C^*)}}$, we shift ec_{r_i} to the place for ec_{r_1+k}, where
      $$k = (r_i - r_1) * [(n - N + (C^* - C)) - r_1]/[(r_l - C^* + 1) - r_1].$$
      - For each of $ec_{r_{(l-C^*+2)}}$,...,ec_{r_l}, we shift ec_{r_i} to the place for ec_{r_l-k}, where
      $$k = (r_l - r_i) * [r_l - (n - N + (C^* - C))]/[r_l - (r_l - C^* + 1)].$$

      This stage is illustrated in Figure 3.4.

2. The new simplification cost for each of these shifted edge collapses ec_{r_1},...,ec_{r_l} will be the cost of the edge collapse at the shifted place. For example, if ec_{r_i} is shifted to the place of ec_{r_j}, the cost of ec_{r_i} will be the cost of ec_{r_j}.

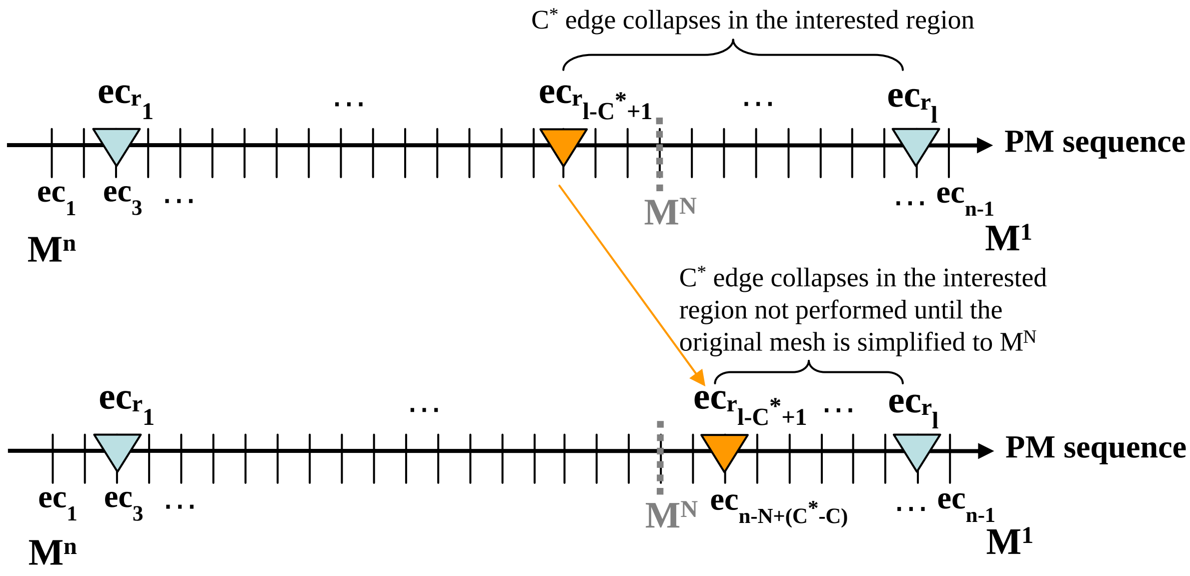

Figure 3.3: Illustration of the first step in the weighting scheme.

Figure 3.5 depicts an example for the proposed weighting scheme, in which n is 36, N is 10, l is 8, C is 3 and C^* is 5. In the first stage, we shift $ec_{r_4}(= ec_{r_{(l-C^*+1)}})$, marked as the orange triangular dot, to the place for $ec_{28}(= ec_{n-N+(C^*-C)})$. In the second stage, all edge collapses ec_{r_1}, ec_{r_2}, ec_{r_3}, ec_{r_5}, ...,ec_{r_8} are shifted as well. Take $ec_{r_2}(= ec_8)$ as an example, the offset k coefficient is computed as $(8-4)*[28-4]/[20-4] = 4*1.5 = 6$, so its shifted place is at $ec_{4+6} = ec_{10}$. Consider another example $ec_{r_7}(= ec_{29})$, the offset k is computed as $(34-29)*[34-28]/[34-20] = 5*0.43 = 2$, so its shifted place is at $ec_{34-2} = ec_{32}$.

When the weighting is applied to more than one region simultaneously, the effect of weighting in each region would be less accurate because the shifted edge collapses for one region may conflict with the shifted edge collapses for another region. We take this issue into account in the re-simplification process. Once edge collapses $ec_{r_{(l-C^*+1)}}$,...,ec_{r_l} are shifted to appropriate places after the weighting scheme is applied in a region, they will not be performed in subsequent applications of weighting scheme in other regions unless the expected simplification target cannot be reached. When this happens, the prohibited edge collapses will be performed until the simplification target is reached.

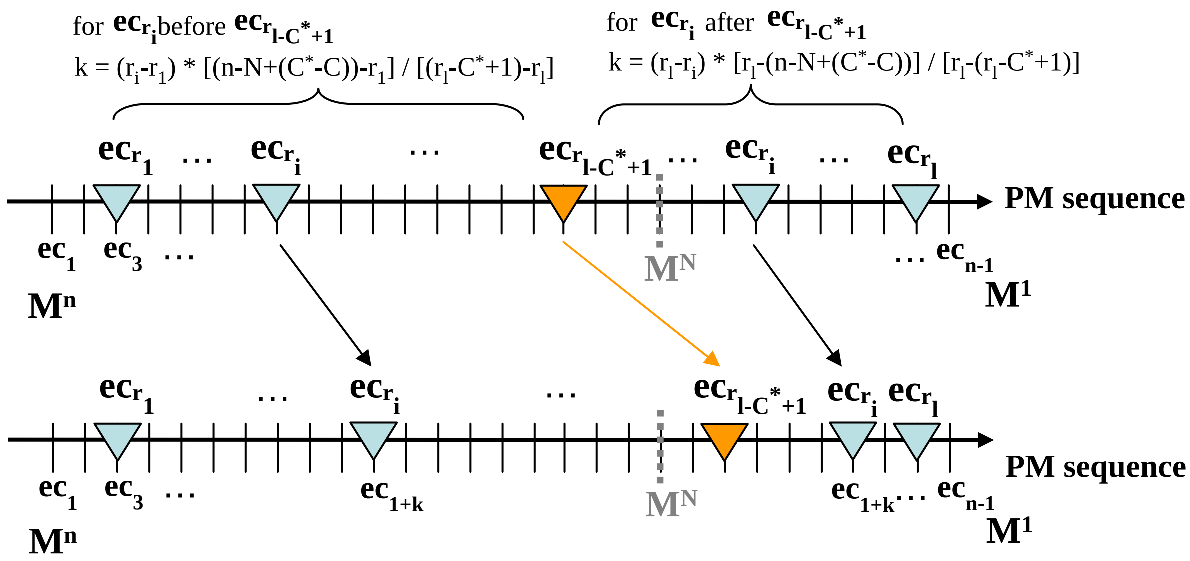

Figure 3.4: Illustration of the second step in the weighting scheme.

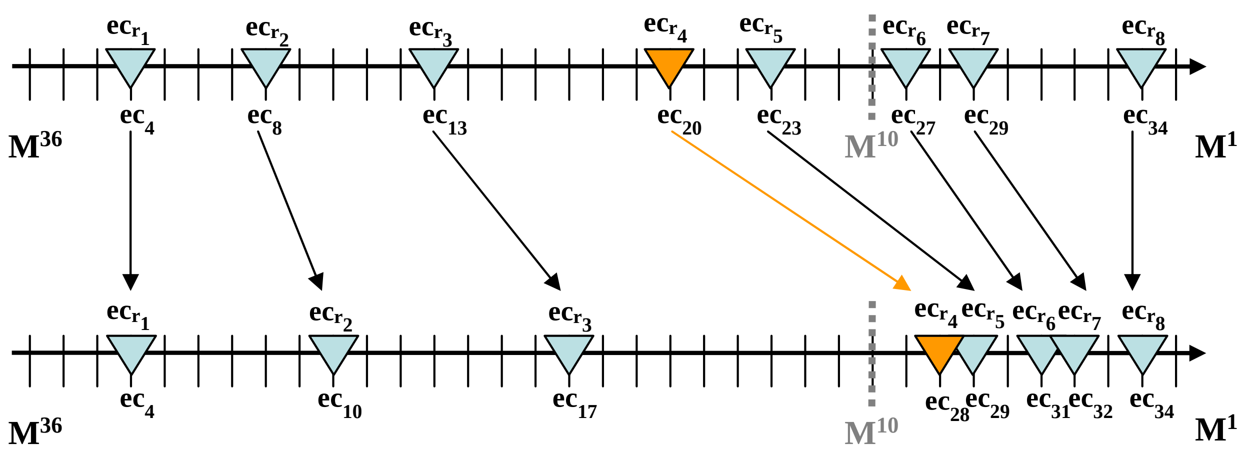

Figure 3.5: An example of weighting.

3.3 Local Refinement

The basic concept of local refinement scheme is to locally refine the interested region by moving down along the active cut of the vertex hierarchy and in the mean time moving up along the active cut to keep polygon count fixed.

We mentioned the vertex splits dependency problem in section 2.4.1, which means that before doing a vertex split, several additional vertex splits may need to be executed due to dependency. Such behavior is not accepted for local refinement because more vertex splits lead to more edge collapses on other regions. In our implementation the vertex split dependency problem is resolved by strategies adapted from Kim's approaches [13].

After local refinement, the costs on the refined regions are relatively lower, so during the subsequent local refinements the refined regions may soon be simplified. We shall adjust the costs on the refined regions to avoid such problem.

As shown in Figure 3.6, one way to avoid this problem is to level the cost distribution over the active cut such that costs assigned to those vertices newly splitted from a vertex v in the local refinement process to be above the cost of v. Moreover, it is desirable to preserve the difference in original costs for nodes in the subtree rooted at v.

To fulfill the above expectations, we prepare an *collapse candidate list* for each subtree rooted at some vertices splitted in the local refinement process, which enlists every executable edge collapses in the subtree. By leveling the costs of records in this list to be above the cost of the subtree's root, the cost distribution over the active cut of the subtree can be leveled as well.

The collapse candidate list is updated only when a vertex is splitted from the root of the subtree, as follows:

- The corresponding edge collapse of this newly performed vertex split is inserted into the collapse candidate list.
- The edge collapse which collapses the vertex is removed from the collapse candidate list (if it exists in the list).

Afterwards, the costs of every edge collapse records in the collapse candidate list are updated as follows:

- Find the record with the smallest original cost among all the records in the list, denote this record as S.

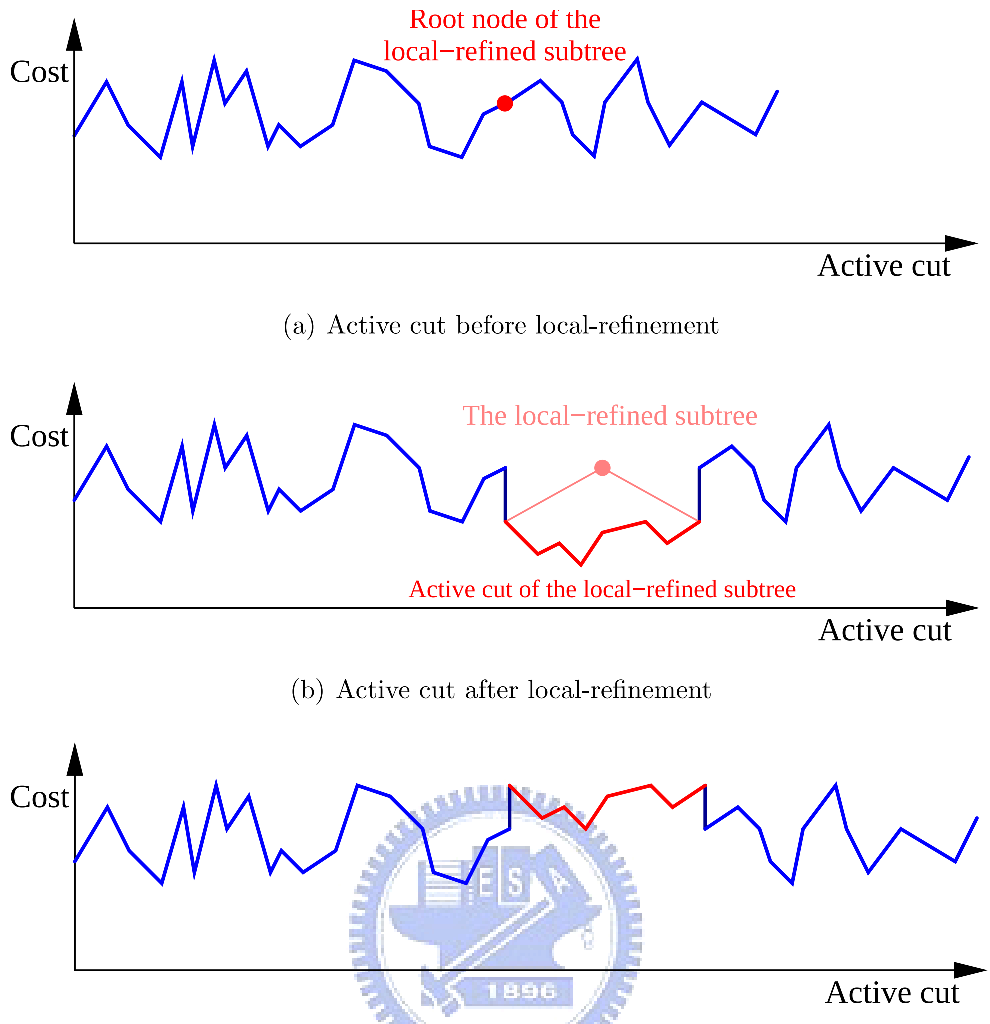

(a) Active cut before local-refinement

(b) Active cut after local-refinement

(c) Active cut after cost adjustment

Figure 3.6: The concept of our cost adjustment scheme.

- Set the cost of S to be the cost of the subtree's root.
- For other records in the collapse candidate list, we set the cost of $record_i$ as the cost of the subtree's root + the difference of original cost between $record_i$ and S.

Figure 3.7 demonstrates the changes of costs in the vertex hierarchy during the cost adjusting process. In Figure 3.7(a)) the vertex hierarchy before local refinements is shown, each box represent a vertex, and the number in it represent the cost of the vertex to be splitted (empty if the vertex is not splittable). In Figure 3.7(b), vertex #2 has just been splitted, and it will be the root of a new cost-adjusted subtree in the local refinement process. In Figure 3.7(c), vertex split #3 has just been executed, the collapse candidate list is updated by adding vertex split #3 into the list and remove vertex split #2 from the list, and the cost of vertex split #3 is set to be the cost of the root (70). In Figure 3.7(d), we first update the cost of the record with smallest original cost (vertex split #4) as the cost of the subtree's root (70), and update the cost of the other record (vertex . In Figure 3.7(e), Figure 3.7(f) and Figure 3.7(g), the costs of records in the cut list are adjusted using our cost adjusting scheme.

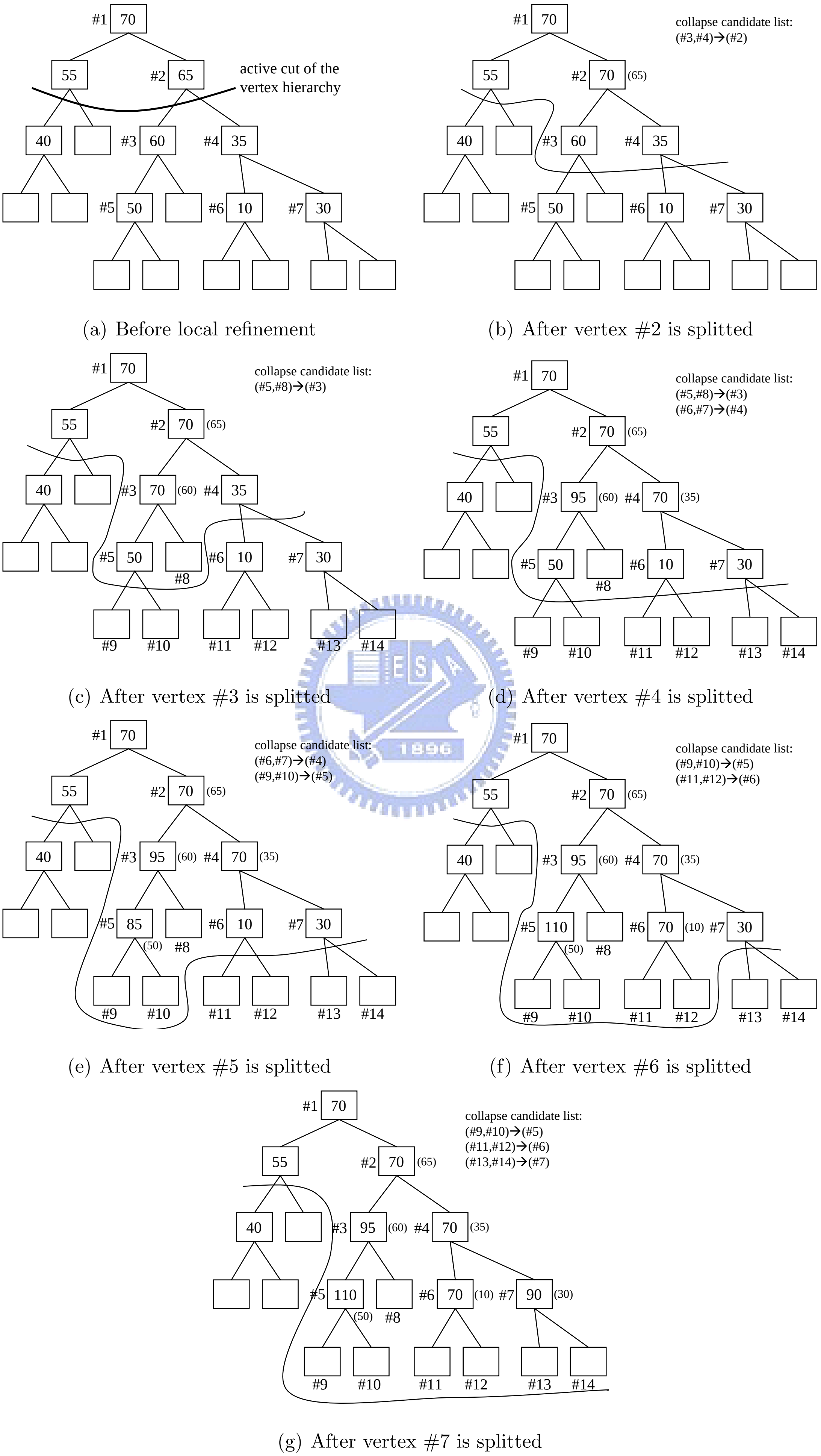

(a) Before local refinement

(b) After vertex #2 is splitted

(c) After vertex #3 is splitted

(d) After vertex #4 is splitted

(e) After vertex #5 is splitted

(f) After vertex #6 is splitted

(g) After vertex #7 is splitted

Figure 3.7: The changes of costs in the vertex hierarchy during the cost adjusting process.

CHAPTER 4

Experimental Results

In this chapter, experimental results of our works will be given. In the first subsections, we will perform tests for the weighting approach, and in the second subsection, tests for the local refinement approach are performed. In the third subsection, comparisons between weighting and local refinements are given. And in the last subsection, we will demonstrate using our two-staged approach to improve the quality of simplified meshes.

We use three models for testing, the first model is Armadillo with 10002 vertices and 20000 faces, which has surface details on some regions as well as some sharp features. The second model is Liberty with 17636 vertices and 35176 faces, which has one important sharp feature (the spikes on her crown) and surface details on some regions. The third model is Parasaur with 3870 vertices and 7685 faces, which has texture information. These models are shown in Figure 4.1.

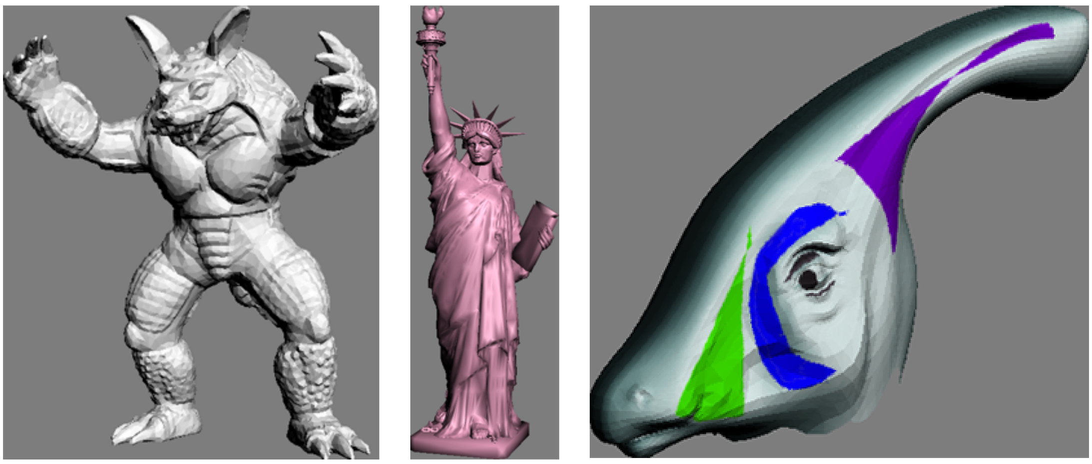

(a) Armadillo (b) Liberty (c) Parasaur

Figure 4.1: The testing models.

All tests are performed on a PC with AMD Athlon 3000+ CPU and 512MB of RAMS and Geforce 6800 graphics card.

4.1 Weighting Tests

Figure 4.2 and figure 4.3 illustrates the result of the armadillo model simplified to $1,000$ polygons using different weighting conditions. The weighting is applied on the face of the armadillo model, and the remaining vertex count are 45, which is the unrefined case, 120, 180, and 300 vertices, as shown in figure 4.2(b)-(e), and figure 4.3 shows the quality of overall model. The effect of weighting is proportional to the number of remaining vertices in the weighted region, and the additional edge collapses on the unweighted regions are scattered evenly, so that the sacrifice of quality is barely visible. Table 4.1 lists the geometric errors of the unweighted and weighted simplifications relative to the original mesh. The errors are measured using Metro [2].

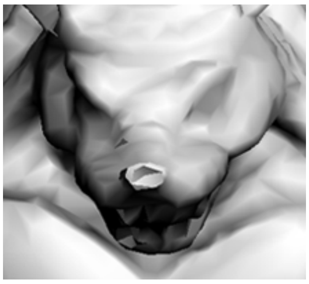

(a) Original mesh, weighting is applied on the facial region

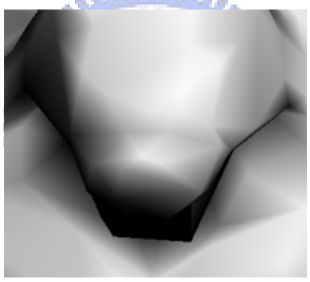

(b) Unrefined simplified mesh (45 vertices remain)

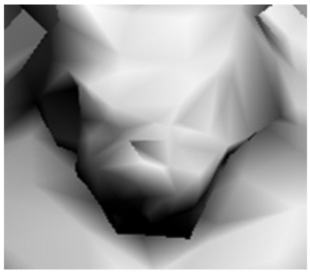

(c) Weighted simplified mesh (120 vertices remain)

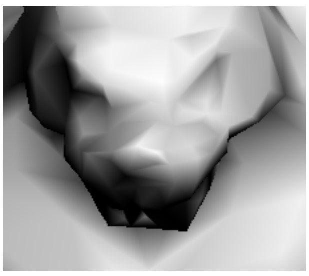

(d) Weighted simplified mesh (180 vertices remain)

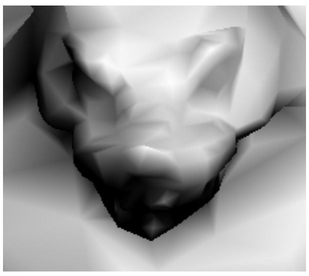

(e) Weighted simplified mesh (300 vertices remain)

Figure 4.2: The quality improvement on weighted regions of Armadillo's simplification.

We also perform the above weighting tests on the simplification result of the Liberty model with 1000 faces, which are shown in Figure 4.4 and Figure 4.5, and similar results

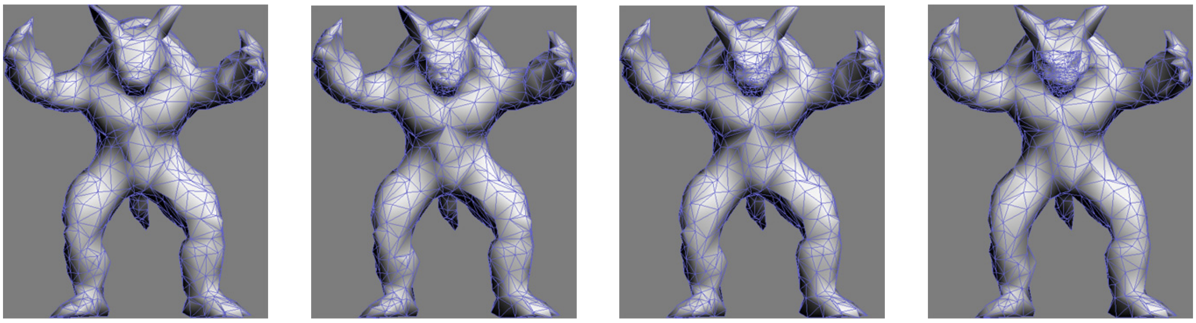

(a) Unrefined simplified mesh, front (b) Weighted simplified mesh (120 vertices), front (c) Weighted simplified mesh (180 vertices), front (d) Weighted simplified mesh (300 vertices), front

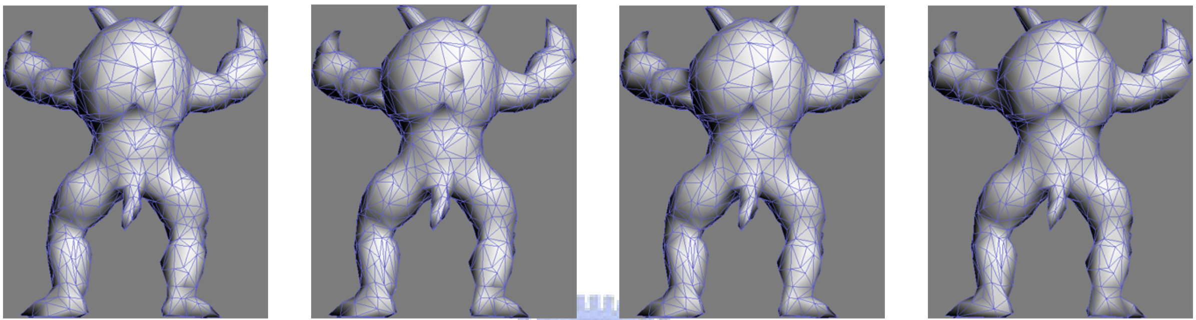

(e) Unrefined simplified mesh, back (f) Weighted simplified mesh (120 vertices), back (g) Weighted simplified mesh (180 vertices), back (h) Weighted simplified mesh (300 vertices), back

Figure 4.3: The sacrifice of quality on unweighted regions of Armadillo's simplification.

	global error	local error
unweighted simplification	0.8156	1.6774
weighted simplification, remaining vertices = 120	0.8137	1.5785
weighted simplification, remaining vertices = 180	0.8513	1.5746
weighted simplification, remaining vertices = 300	1.0891	1.1065

Table 4.1: Comparing geometric errors of Armadillo's weighted simplification with 2000 faces

are claimed. Table 4.2 lists the geometric errors of the unweighted and weighted simplifications relative to the original mesh. The global error measures the geometric difference of the entire mesh and the local error focus on the regions where weightings are applied. The local error reduces when the remaining vertex count of weighted region increases while the global error arises. Since most of the errors are introduces to the regions we do not interested, and thus can be discarded.

Figure 4.6 shows the result of simplifying to $1,000$ polygons with multiple weightings.

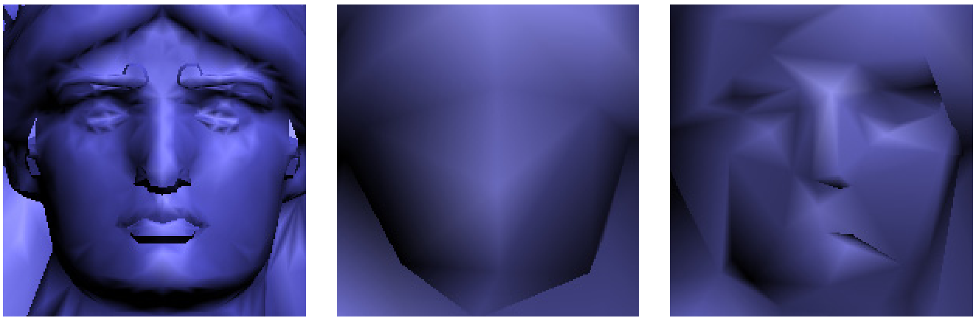

(a) Original mesh, weighting is applied on the facial region (b) Unrefined simplified mesh (10 vertices remain) (c) Weighted simplified mesh (60 vertices remain)

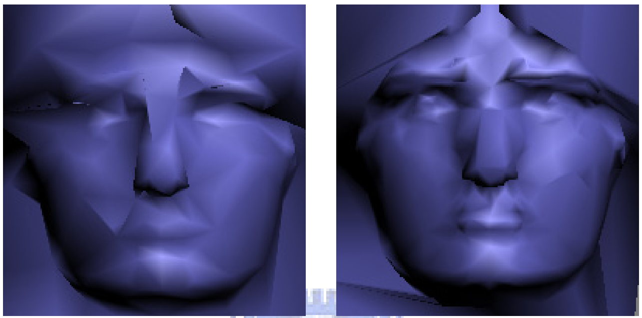

(d) Weighted simplified mesh (180 vertices remain) (e) Weighted simplified mesh (360 vertices remain)

Figure 4.4: The quality improvement on weighted regions of Liberty's simplification.

	global error	local error
unweighted simplification	18.0879	1.6528
weighted simplification, remaining vertices = 60	18.0878	1.3043
weighted simplification, remaining vertices = 180	18.0877	0.8865
weighted simplification, remaining vertices = 300	18.0832	0.7985

Table 4.2: Comparing geometric errors of Liberty's weighted simplification with 1000 faces

The effects of these three weightings will be blended to produce the final result. Regions without weighting can also be preserved well.

To find the effect of weighting on simplifications not at the weighting's default simplification ratio, we apply weighting on the facial region of Armadillo's simplification with 1000 faces, then we generate simplifications at other ratios using the weighted PM sequence. The testing results are shown in table 4.3, in which each row shows the number of vertices on the selected region before and after weighting on simplification with a specific simplification ratio, and comparisons between the unrefined simplifications and the simplifications generated from the above weighted PM sequence are shown in Figure 4.7. We find that effect of weighting is equally effective on simplifications with lower ratios then the default one (500 and 250 faces), but is less effective on simplifications with higher ratios (2000, 4000, 6000, 8000, 10000, 15000 faces).

face count	vertices count before weighting	vertices count after weighting	increased vertices count respect to the face count
250	3	34	0.124
500	9	72	0.126
1000 (default)	17	148	0.131
2000	34	159	0.0625
4000	69	191	0.0305
6000	115	214	0.0165
8000	140	237	0.0121
10000	189	260	0.0071
15000	286	325	0.0026

Table 4.3: The effect of weighting on simplifications with default and non-default ratios

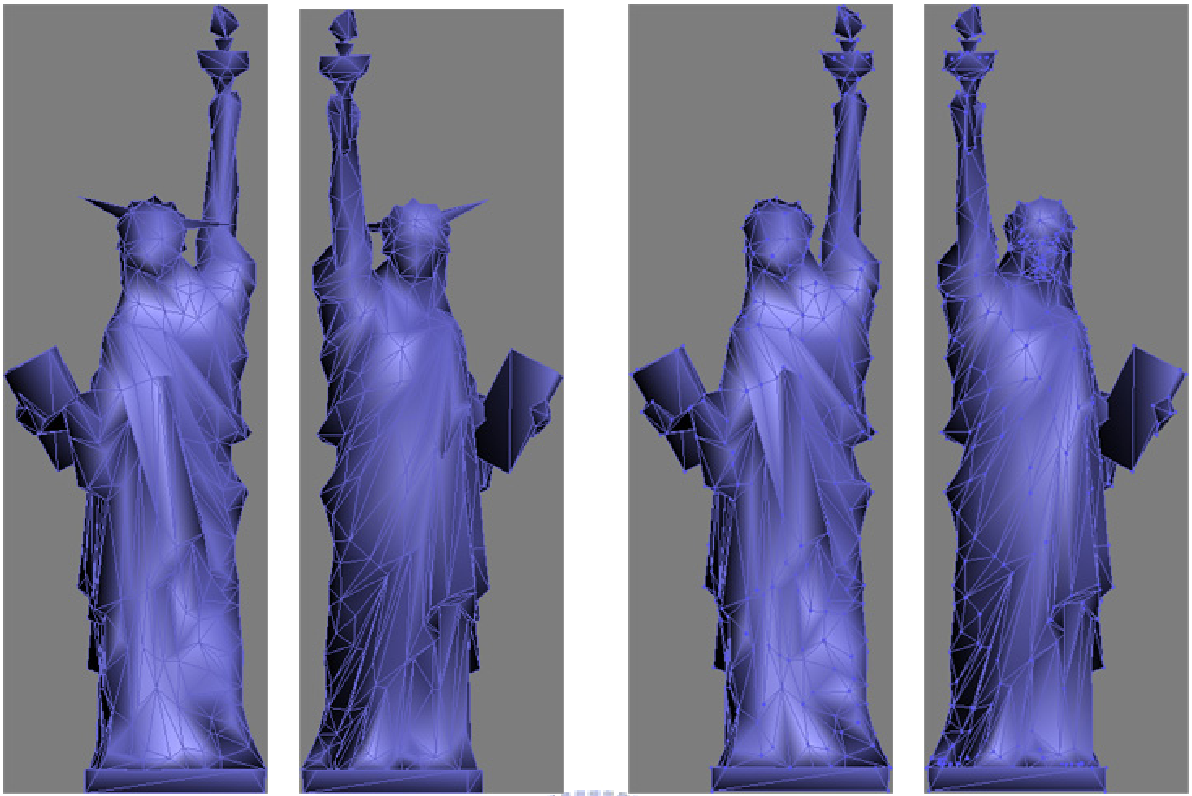

(a) Unrefined simplified mesh, front (b) Unrefined simplified mesh, back (c) Weighted simplified mesh (60 vertices), front (d) Weighted simplified mesh (60 vertices), back

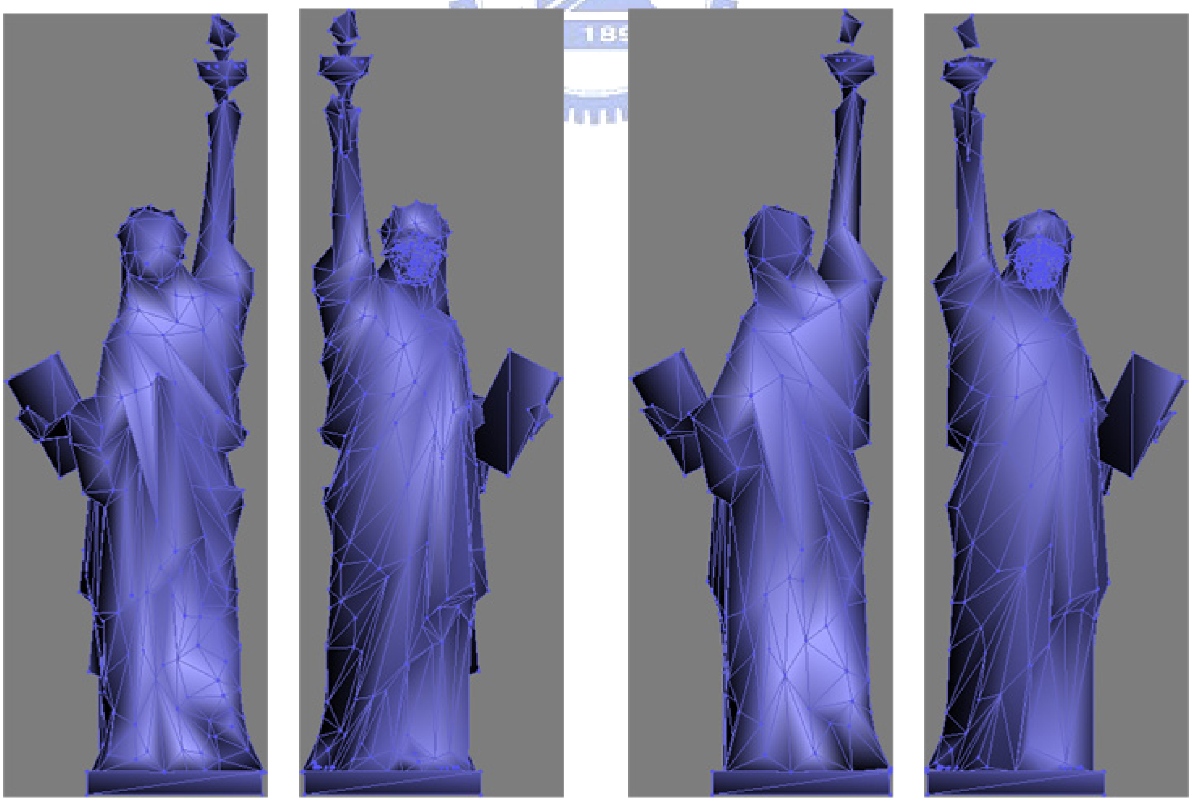

(e) Weighted simplified mesh (180 vertices), front (f) Weighted simplified mesh (180 vertices), back (g) Weighted simplified mesh (300 vertices), front (h) Weighted simplified mesh (300 vertices), back

Figure 4.5: The sacrifice of quality on unweighted regions of Liberty's simplification.

(a) First weighting (b) Second weighting (c) Third weighting (d) Apply the three weightings simultaneously

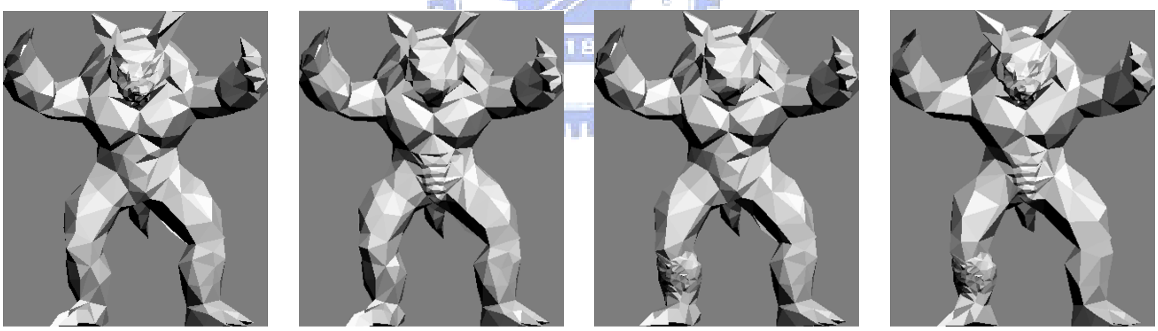

(e) First weighting applied (f) Second weighting applied (g) Third weighting applied (h) Three weightings applied simultaneously

Figure 4.6: Effects of multiple weighting.

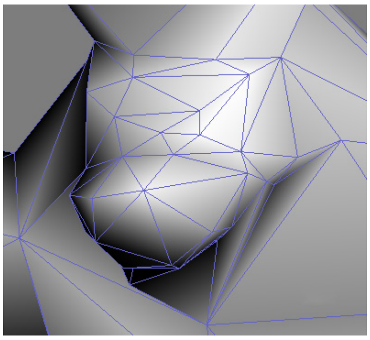

(a) simplification with 250 faces, weighted

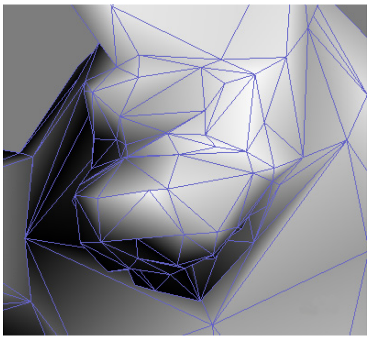

(b) simplification with 500 faces, weighted

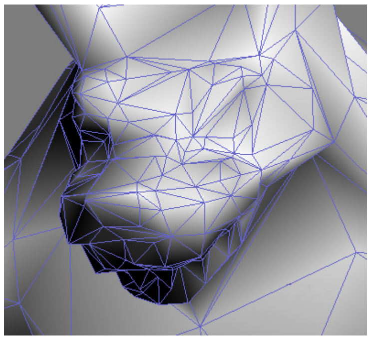

(c) simplification with 1000 faces (default), weighted

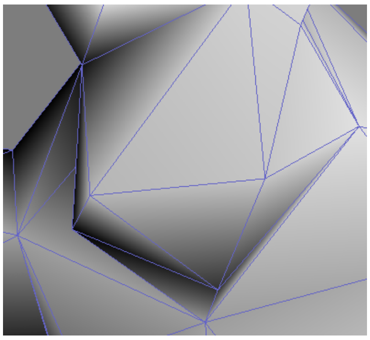

(d) simplification with 250 faces, unrefined

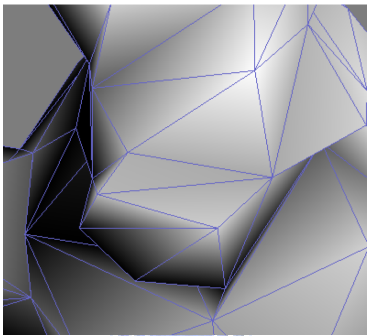

(e) simplification with 500 faces, unrefined

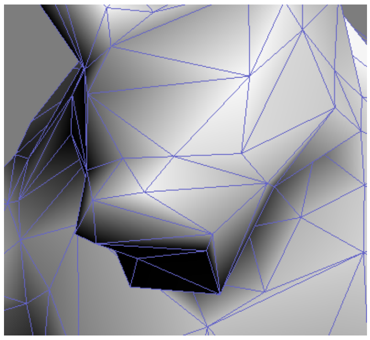

(f) simplification with 1000 faces, unrefined

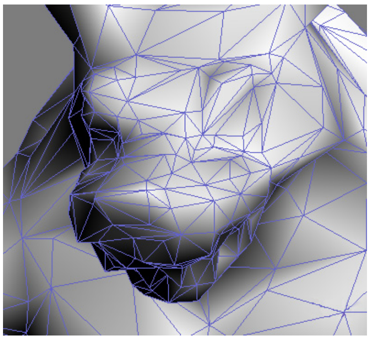

(g) simplification with 2000 faces, weighted

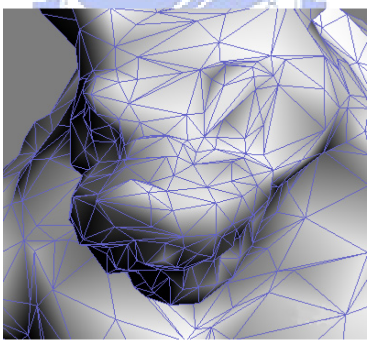

(h) simplification with 4000 faces, weighted

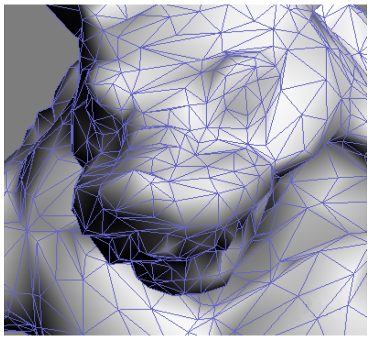

(i) simplification with 8000 faces, weighted

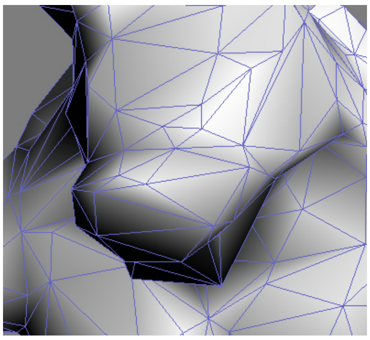

(j) simplification with 2000 faces, unrefined

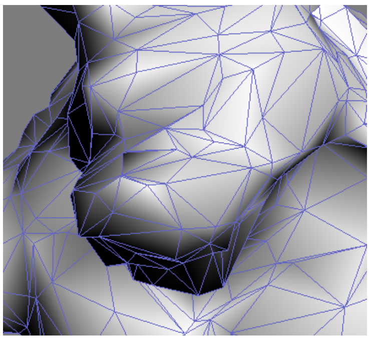

(k) simplification with 4000 faces, unrefined

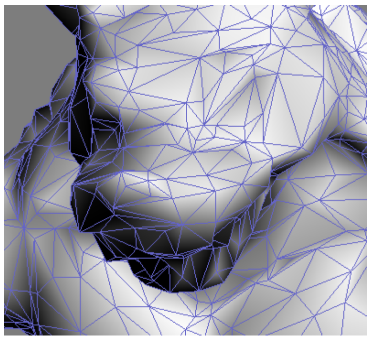

(l) simplification with 8000 faces, unrefined

Figure 4.7: The effect of weighting on simplifications with default and non-default ratios.

4.2 Local Refinement Tests

First we demonstrate the effect of cost adjustment for the cost distribution over the entire mesh in Figure 4.8. Figure 4.8(a) shows the original cost distribution over the entire simplified mesh of Armadillo with 1000 faces. In Figure 4.8(b) the cost distribution after local refinement but without cost adjusting is shown, and we can see that the local-refined regions (marked as red segments) have significantly lower cost than other regions. And Figure 4.8(c) shows the the cost distribution after local refinement with cost adjusting. We can see that with cost adjusting scheme the costs on the local-refined regions are leveled up to match the cost distributions over the entire mesh.

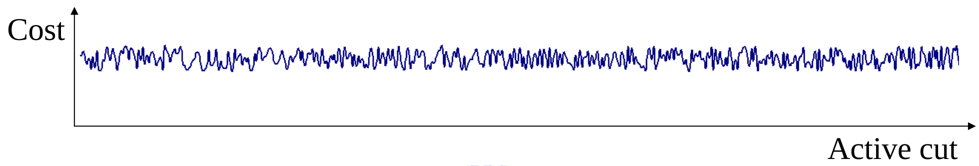

(a) original cost distribution over the entire simplified mesh

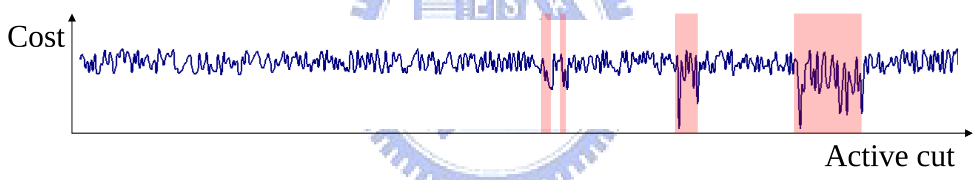

(b) cost distribution after local refinement without cost adjusting

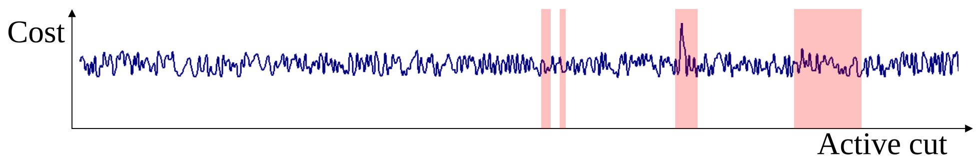

(c) cost distribution after local refinement with cost adjusting

Figure 4.8: The effects of cost adjusting for the cost distribution over the entire mesh.

Local refinement requires users to select a small region of surface mesh to be refined, and and the refine process is proceeded iteratively until satisfy. Figure 4.9 illustrates a small region of simplified mesh of $1,000$ faces with and without refined, and table 4.4 is the geometric error after each refinement iteration. The more iteration step, the better geometric features can be preserved, and affect less to the other regions than the weighting approach.

To demonstrate the effect of cost adjustments implemented in our local refinement

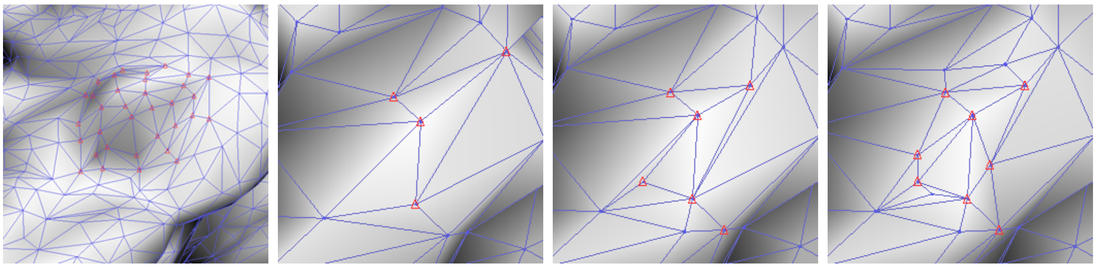

(a) The region to be refined on the original mesh (b) Unrefined simplification (c) After 1 iteration (4 vertex splits are performed) (d) After 2 iteration (10 vertex splits are performed)

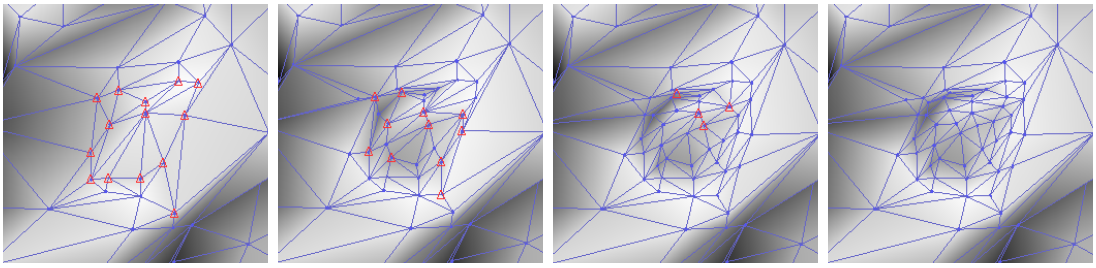

(e) After 3 iteration (18 vertex splits are performed) (f) After 4 iteration (32 vertex splits are performed) (g) After 5 iteration (43 vertex splits are performed) (h) After 6 iteration (47 vertex splits are performed)

Figure 4.9: Using local refinement to gradually refine Armadillo's left eye.

	global error	local error
unrefined simplification	1.3924	1.1964
after 1 iteration	1.3925	1.1203
after 2 iterations	1.3957	0.5284
after 3 iterations	1.3958	0.5338
after 4 iterations	1.3958	0.3578
after 5 iterations	1.3957	0.3515
after 6 iterations	1.3958	0.3521

Table 4.4: Geometric errors of performing local refinements on the left eye of the Armadillo model

approach, we show the locations of edge collapses executed by three consecutive local refinements with and without cost adjustments applied on the Armadillo model's simplification with 1000 faces in Figure 4.10. The refined region of each local refinement is marked as red dots and the edge collapses executed by each local refinements are marked as green dots. We find that without cost adjustments, the refined regions of earlier local refinements are likely to be collapsed by later local refinements, but with cost adjustments enabled the above problem is solved.

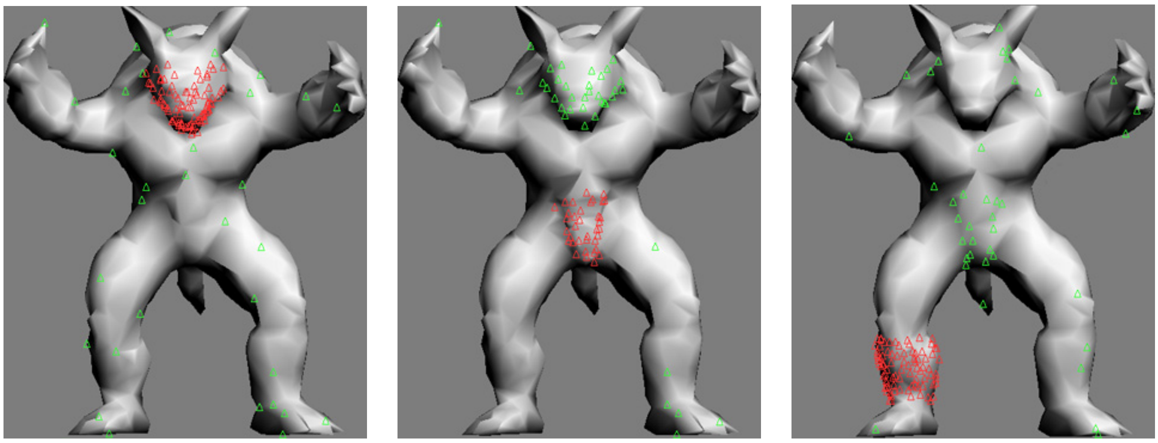

(a) First local refinement applied without cost adjustment (b) Second local refinement applied without cost adjustment (c) Third local refinement applied without cost adjustment

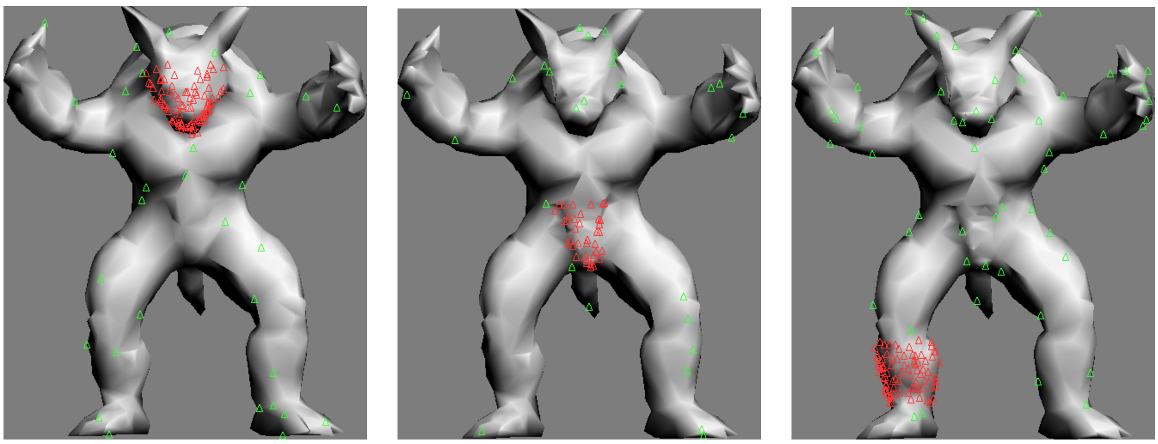

(d) First local refinement applied with cost adjustment (e) Second local refinement applied with cost adjustment (f) Third local refinement applied with cost adjustment

Figure 4.10: Edge collapses executed by local refinements with and without cost adjustments.

4.3 Comparisons of Weighting and Local Refinements

Both weighting and local refinement have their own strength and weakness, in this section, we will try to compare these two methods in several aspects.

Figure 4.11 demonstrates the simplification results of refining the facial region of Armadillo model's simplification with 1000 faces using weighting, local refinements, and combining both methods, and table 4.5 lists the geometric error of Figure 4.11. Same numbers of vertices are added on the facial region by the three methods, for example, in Figure 4.11(a) 162 additional vertices are allocated by weighting, in Figure 4.11(b) 162 vertex splits are performed by local refinements, and in Figure 4.11(c) first 73 additional vertices are allocated by weighting, followed by 90 vertex splits performed by local refinements. We find that the refining effect of weighting is concentrated on the selected region only, while the refining effect of local refinements tends to span across the selected region and effect the nearby unselected regions as well. This is because local refinement is based on the pre-built vertex hierarchy, so that to execute a vertex split on the selected region, more vertex splits may be executed due to parent-children dependencies in the vertex hierarchy. According to table 4.5, the refining effect of combining both methods is better then weighting and local refinements. The reason is that after weighting a better structured vertex hierarchy is formed, so the effect of local refinements could be more concentrated on the facial region, which results in less local and global errors.

	global error	local error
unrefined simplification	0.8018	1.4721
refined by weighting	1.2584	1.2214
refined by local refinements	1.4717	1.1045
refined by both	1.2583	0.7295

Table 4.5: Geometric errors on Armadillo's refined simplifications by weighting, local refinements and both

We now compare the ability to recover sharp features using weighting and local refinements. Figure 4.12 shows the results of using weighting to recover the spikes on the Liberty model's simplification with 500 faces. Even we specify that all vertices on the spikes (marked as red dots in Figure 4.12(a)) shall remain after weighting, the shape of the sharp features is still not preserved well. On the other hand, the spikes can be recovered after performing three iterations of local refinements on them, as shown in Figure 4.13.

In Figure 4.14 and Figure 4.15, results of using weighting and local refinements to recover the spikes on the Liberty model's simplification with 1000 faces are shown. As shown in Figure 4.15, the spikes can be recovered after performing just one iteration of local refinement on them, with 7 additional vertices allocated on the refined region. But if we use weighting to recover the spikes with the budget of 7 additional vertices, the spikes cannot be recovered well, as shown in Figure 4.14(c). In fact, we have found that at least 11 additional vertices are required for weighting to recover the spikes, as shown in 4.14(d).

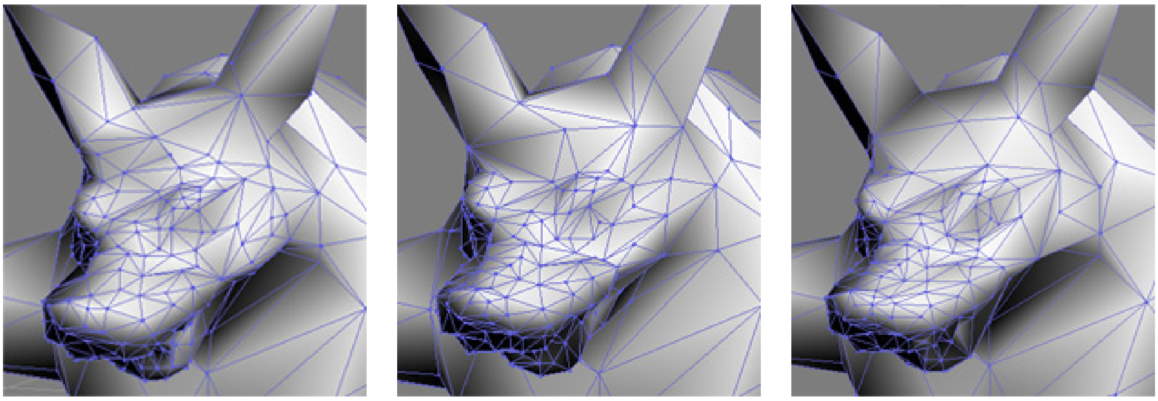

(a) Refined simplification by local refinements, facial region (b) Refined simplification by weighting, facial region (c) Refined simplification by combining both methods, facial region

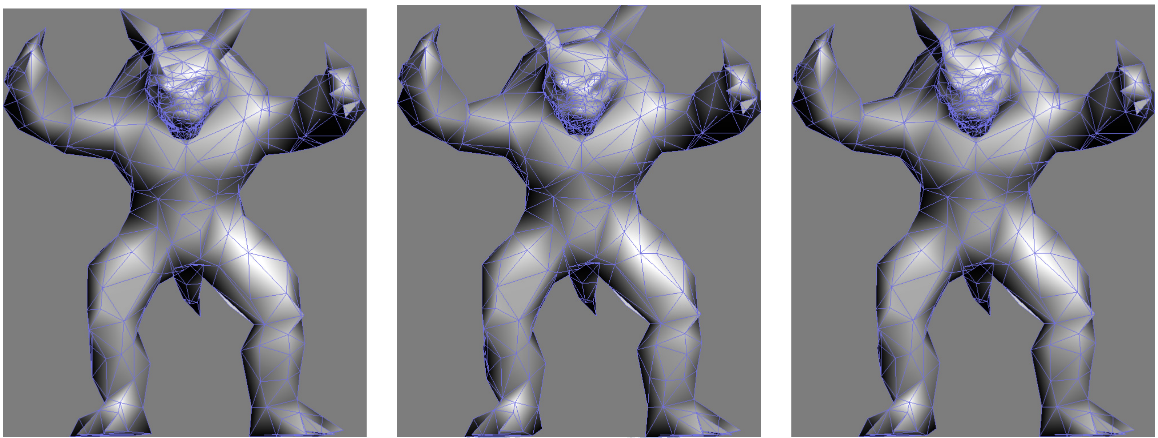

(d) Refined simplification by local refinements, front (e) Refined simplification by weighting, front (f) Refined simplification by combining both methods, front

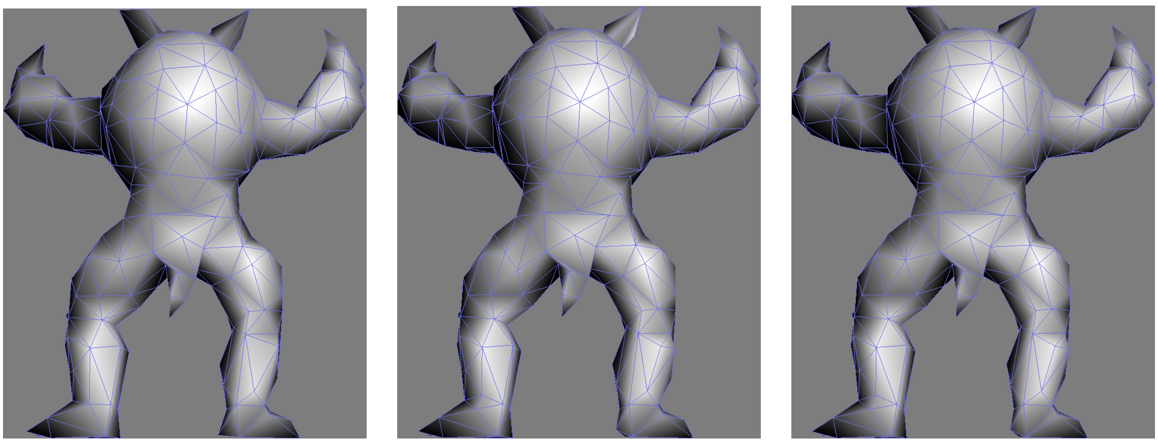

(g) Refined simplification by local refinements, back (h) Refined simplification by weighting, back (i) Refined simplification by combining both methods, back

Figure 4.11: Comparing the refined simplifications by weighing, local refinements and both.

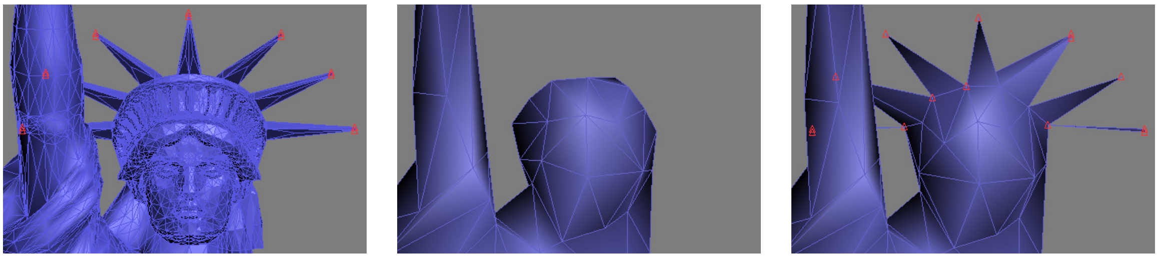

(a) Weighted region on the original mesh.

(b) Unweighted simplification.

(c) Weighted simplification.

Figure 4.12: Recover sharp features on the Armadillo's simplification with 500 faces by weighting.

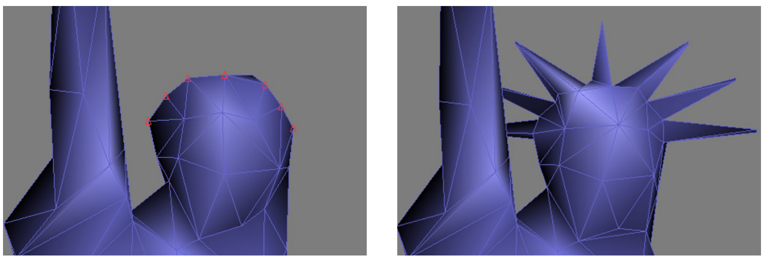

(a) Select vertices near the missing spikes.

(b) Result after three iteration of local refinement.

Figure 4.13: Recover sharp features on the Armadillo's simplification with 500 faces by local refinements.

(a) Weighted region on the original mesh.

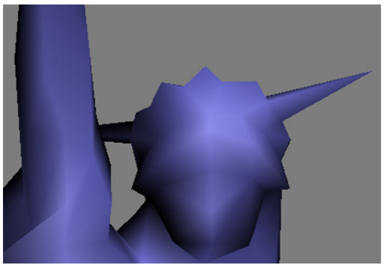

(b) Unweighted simplification.

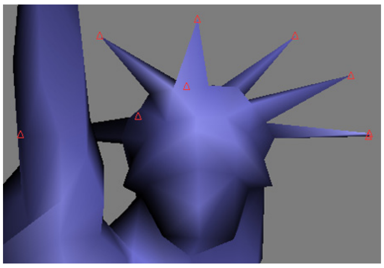

(c) Weighted simplification, 7 vertices are added on the weighted region.

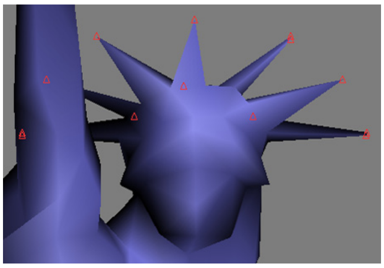

(d) Weighted simplification, 11 vertices are added on the weighted region.

Figure 4.14: Recover sharp features on the Armadillo's simplification with 1000 faces by weighting.

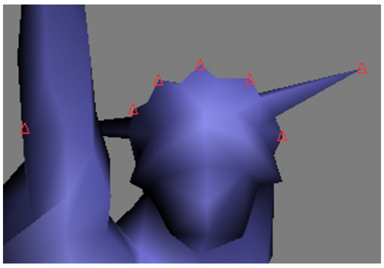

(a) Select vertices near the missing spikes.

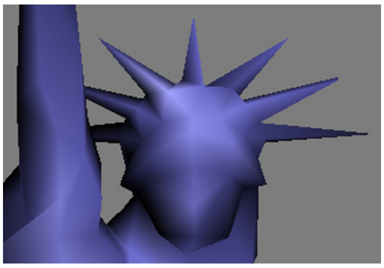

(b) Result after one iteration of local refinements.

Figure 4.15: Recover sharp features on the Armadillo's simplification with 1000 faces by local refinements.

4.4 Case Studies

In this section, we will demonstrate using our two-staged approach to refine the simplifications of three different testing models.

4.4.1 Case1: Armadillo

In this subsection, we try to refine the simplification with 1000 faces of the Armadillo model produced by QEM using the proposed two-stage approach. We use weighting to improve the quality on the facial and torso regions and use local refinements to further refine the eyes. The comparisons between the original mesh, the unrefined simplification and the refined simplification are shown in Figure 4.16. In Figure 4.17, we can see the huge quality improvement on the facial and torso regions.

The geometric errors of the unrefined and refined simplifications are shown in table 4.6. While the global error increases after the refinement process because sacrifice of quality was done on unrefined regions, the local errors on the semantically important regions decrease considerably after refinement was applied.

	global error	local error
unrefined simplification with 1000 faces	0.8018	2.4510
refined simplification with 1000 faces	1.1427	1.0239

Table 4.6: Comparing geometric errors of Armadillo's unrefined and refined simplifications

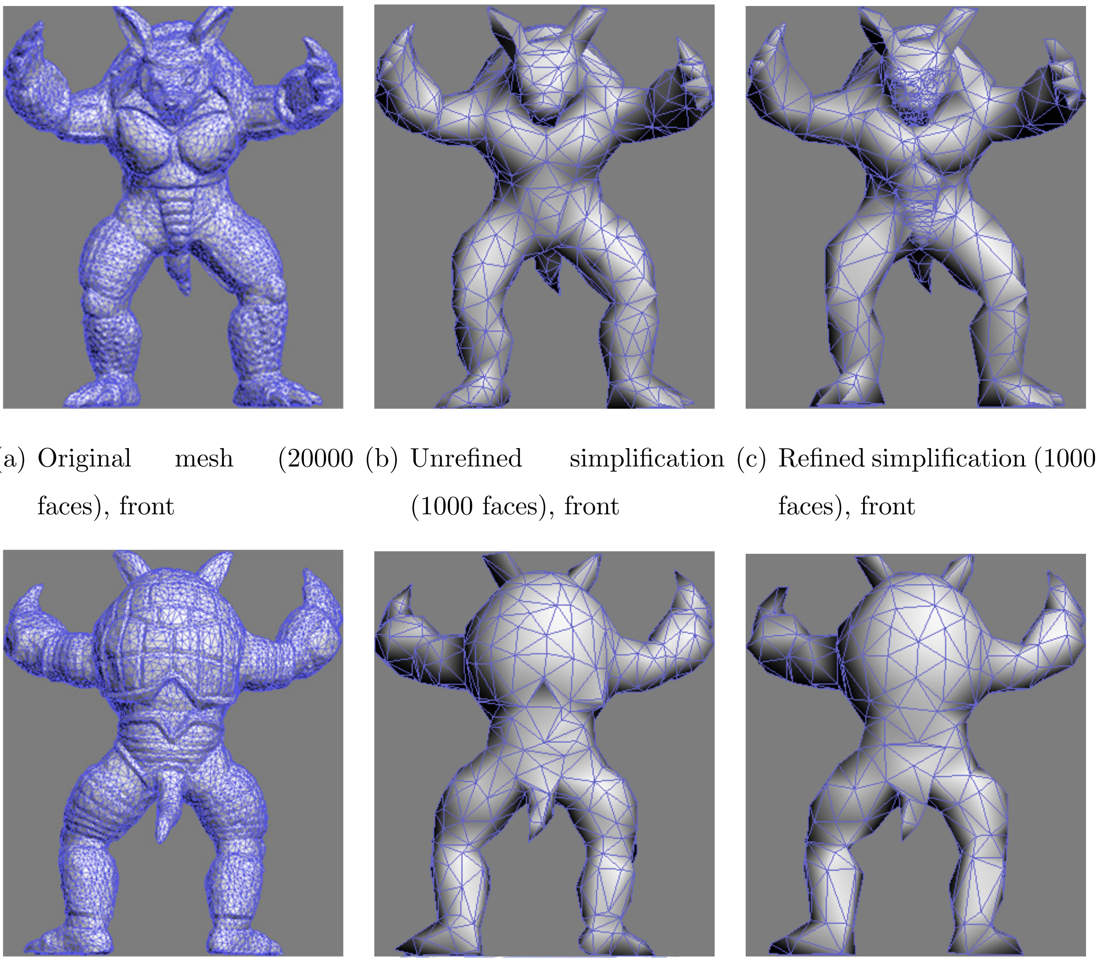

(a) Original mesh (20000 faces), front (b) Unrefined simplification (1000 faces), front (c) Refined simplification (1000 faces), front

(d) Original mesh (20000 faces), back (e) Unrefined simplification (1000 faces), back (f) Refined simplification (1000 faces), back

Figure 4.16: Comparison of the unrefined and the refined simplifications with 1000 faces of Armadillo.

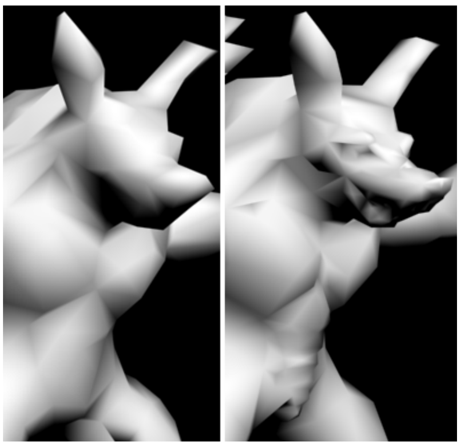

Figure 4.17: Closer comparisons between the unrefined (left) and refined (right) simplifications with 1000 faces of Armadillo.

4.4.2 Case2: Liberty

The second test case is the Liberty model's simplification with 1000 faces produced by QEM. We use weighting to refine the face, torch and foots, and use local refinement to recover the spikes on the crown. The refined simplification and its comparison with the unrefined version and the original mesh are shown in figure 4.18.

Again we use Metro [2] to measure the geometric errors of the unrefined and refined simplifications, as shown in table 4.7. We find that there is no significant difference between the global geometric errors of unrefined and refined simplification, but the local errors on the refined regions are decreased.

	global error	local error
unrefined simplification with 1000 faces	18.0879	4.4558
refined simplification with 1000 faces	18.0969	1.8194

Table 4.7: Comparing geometric errors of Liberty's unrefined and refined simplifications

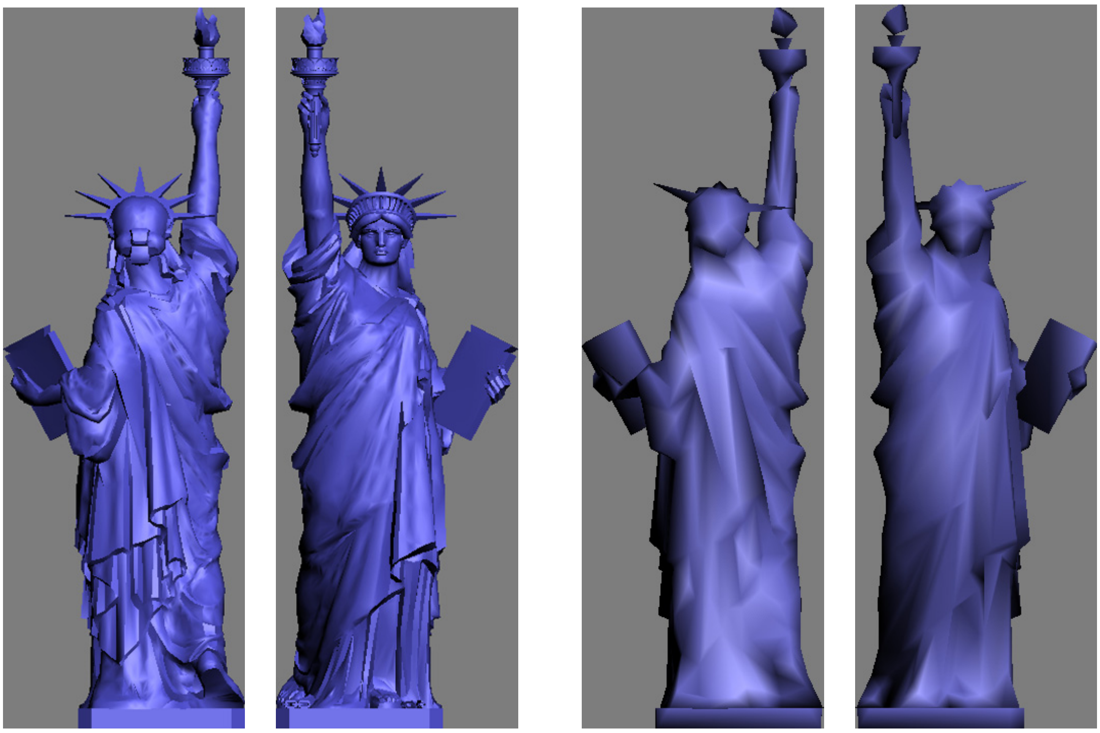

(a) Original mesh (35176 faces), back (b) Original mesh (35176 faces), front (c) Unrefined simplification (1000 faces), back (d) Unrefined simplification (1000 faces), front

(e) Refined simplification (1000 faces), back (f) Refined simplification (1000 faces), front

Figure 4.18: Comparison of the unrefined and the refined simplifications with 1000 faces of Liberty.

4.4.3 Case3: Parasaur

The third test model is Parasaur which has texture information. We choose APS as the simplification algorithm because it is designed for preserving textures, however, the texture quality of Parasaur's simplifications still degrades notably when simplified to very low polygon counts, such as 500 faces. The comparisons between the original mesh, the unrefined simplification and the refined simplification are shown in Figure 4.19.

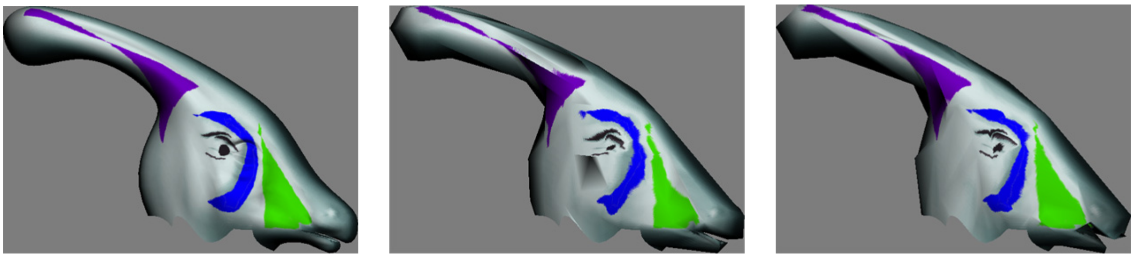

(a) Original mesh (3870 faces), left

(b) Unrefined simplification (500 faces), left

(c) Refined simplification (500 faces), left

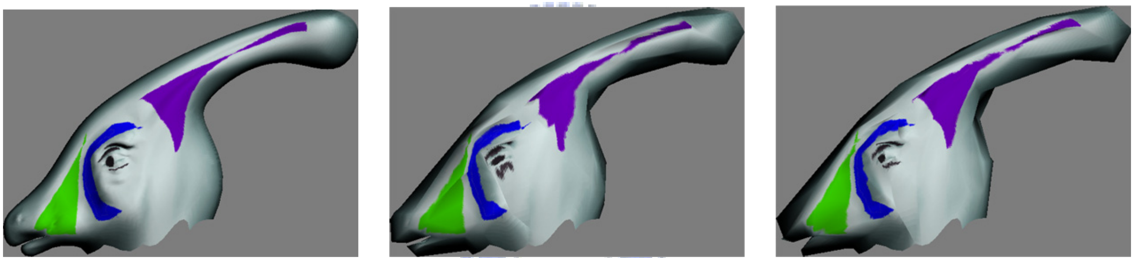

(d) Original mesh (3870 faces), right

(e) Unrefined simplification (500 faces), right

(f) Refined simplification (500 faces), right

Figure 4.19: Comparison of the unrefined and the refined simplifications with 760 faces of Parasaur.

CHAPTER 5

Conclusion and Future Work

5.1 Summary

In this thesis, we propose a two-stage approach for users to refine unsatisfying regions on any levels of simplification. Our approach is especially useful for refining simplifications with low polygon counts.

The first stage is weighting, which allows users to refine large regions on the simplifications. Weighting is done by repositioning edge collapses on the selected regions to later places in the PM sequence. Our weighting approach offers users a precise control over the degree of refinements, is independent on the error metrics, and can be applied to multiple regions.

The second stage is local refinement, which allows users to do fine tuning on the simplified meshes. Local refinement is done by moving up and done along the active cut on the vertex hierarchy. We proposed a cost adjusting scheme to support multiple local refinements, and we solved the vertex split dependency problem by methods adapted from Kim's approaches [13].

5.2 Future work

The first thing about weighting that could be improved is that the user needs to specify a target simplification ratio for the weighting to taking effect, and the effect of weighting is undefined on simplifications not at the target simplification ratio. Therefore we shall redesign the weighting approach so that the effect of weighting is valid on any simplification ratios, or at least valid on some uniformly sampled simplification ratios, such as 50%, 40%, 30%, 20%, 10% and 5%.

Another potential improvement for weighting is that the computation time of weighting can be greatly decreased if we could retrieve the weighted PM sequence by simulating the reordering of edge collapses in the PM sequence directly, instead of using weighting values to bias the PM sequence. In this way, the recomputation of the whole simplification process is avoided.

And for local refinements, two features of the current cost adjusting scheme shall be reexamined. The first feature is that we lift the cost distribution on the cost-adjusted subtree to be just above the cost of the subtree's root node. However, if the cost of the root node is the lowest ones on the entire mesh, the effect of cost adjustment may be ineffective because the cost-adjusted subtree still has lowest costs on the entire mesh. The second feature is that we preserve the cost differences of every nodes on the active cut of the cost-adjusted subtree. However, this may lead to unnecessarily high cost values on the subtree's active cut when the cost of the subtree's root node is already high.

Potential future work for user-assisted mesh simplifications are listed as follows:

- **User-assisted mesh simplification for specific error metrics** Currently our approach is suited for simplifications produced by any error metrics, but it also may be advantageous to develop user-assisted mesh simplification that is designed for specific error metrics, such as APS or IDS. For example, an user-assisted IDS approach may allow users to control the number and positions of sampling view points.

- **User-assisted billboard clouds** Billboard clouds [21] is an approach for extreme mesh simplification, in which 3D models are simplified onto a set of planes with texture and transparency maps. Billboard clouds are generated automatically by an optimization approach which minimizes geometric errors, so unsatisfying results for some users are likely to occur. We think that adapting the concept of user-assistance into billboard clouds can solve such limitations.

Bibliography

[1] M. C. R. C. Cignoni, P. and R.scopigno. Zeta: A resolution modeling system. pages 305–329, 1998.

[2] P. Cignoni, C. Rocchini, and R. Scopigno. Metro: Measuring error on simplified surfaces. *Computer Graphics Forum*, 17(2):167–174, 1998.

[3] J. H. Clark. Hierarchical geometric models for visible surface algorithms. volume 19(10), pages 547–554, 1976.

[4] P. M. DeFloriani, L and E. Puppo. Efficent implementation of multi-triangulations. pages 45–50, 1998.

[5] D. S. Erik Pojar. User-controlled creation of multiresolution meshes. In *Proceedings of the 2003 symposium on Interactive 3D graphics*, pages 127–130, 2003.

[6] M. Garland and P. S. Heckbert. Surface simplification using quadric error metrics. In *SIGGRAPH 97 Conference Proceedings*, pages 209–216, Aug. 1997.

[7] B. W. Gong Li. Semiautomatic simplification. pages 43–48, 2001.

[8] B. Hamann. A data reduction scheme for traingulated surfaces. volume 11, pages 45–50, 1998.

[9] H. Hoppe. Progressive meshes. In *SIGGRAPH 96 Conference Proceedings*, pages 99–108, Aug. 1996.

[10] H. Hoppe. View-dependent refinement of progressive meshes. pages 189–198, July 1997.

[11] T. D. T. D. J. M. Hoppe, H and W. Stuetzle. Mesh optimization. pages 19–26, 1993.

[12] M. O. Jonathan Cohen and D. Manocha. Appearance-preserving simplification. In *Proceedings of SIGGRAPH 98*, 1998.

[13] S. L. Junho Kim. Truly selective refinement of progressive meshes. In *Graphics interface 2001*, 2001.

[14] S. L. Junho Kim. Transitive mesh space of a progressive mesh. In *IEEE Transaction on Visualization and Computer Graphics*, pages 463–480, Dec. 2003.

[15] Y.-C. Liao. *Mesh Simplification with Geometry and Material Preserving*. PhD thesis, National Chiao Tung University, HsinChu, Taiwan, Republic of China, 2004.

[16] Lindstrom and G. Turk. Image-driven simplification. In *ACM Trans. Graphics*, 2000.

[17] D. P. Luebke. A developer's survey of polygonal simplification algorithms. *IEEE Computer Graphics and Applications*, pages 24–35, July 2001.

[18] J. C. M. K. N. Williams, D. Luebke and B. Schubert. Perceptually guided simplification of lit, textured meshes. 2003.

[19] J. Rossignac and P. Borrel. Multi-resolution 3d approximations for rendering complex scenes. pages 455–465, 1993.

[20] J. A. Z. Schroeder, W J and W. E. Lorensen. Decimation of triangle meshes. pages 65–70, 1992.

[21] F. X. S. J. D. Xavier Decoret, Fredo Durand. Billboard clouds for extreme mesh simplification. 2003.

[22] M. G. Youngihn Kho. User-guided simplification. In *Proceedings of the 2003 symposium on Interactive 3D graphics*, pages 123–126, 2003.